LAWRENCE
LIVERMORE
NATIONAL
LABORATORY

LLNL-JRNL-646271

Polycrystal Plasticity: Comparison Between Grain-Scale Observations of Deformation and Simulations

R. Pokharel, J. Lind, A. Kanjarla, R. A. Lebensohn, S. F. Li, P. Kenesei, R. M. Suter, A. D. Rollett

November 18, 2013

Annual Review of Condensed Matter Physics

Polycrystal Plasticity: Comparison Between Grain Scale Observations of Deformation and Simulations

Reeju Pokharel[a,c,*], Jonathan Lind[a], Anand K. Kanjarala[c,e], Ricardo A. Lebensohn[c], Shiu Fai Li[a,b], Peter Kenesei[d], Robert M. Suter[a], Anthony D. Rollett[a]

[a]*Carnegie Mellon University, 5000 Forbes Avenue, Pittsburgh PA 15213, USA*
[b]*Lawrence Livermore National Laboratory, 7000 East Avenue, CA 94550 USA*
[c]*Materials Science and Technology Division, Los Alamos National Laboratory, Los Alamos, NM 87544, USA*
[d]*Advanced Photon Source, Argonne National Laboratory, 9700 South Cass Avenue, Argonne, IL 60439, USA*
[e]*Department of Metallurgical and Materials Engineering, IIT-Madras, Chennai, 60036, INDIA*

Abstract

The response of polycrystals to plastic deformation is studied at the level of variations within individual grains and comparisons are made to theoretical calculations using crystal plasticity. We provide a brief overview of crystal plasticity and a review of the literature, which is dominated by surface observations. The motivating question asks how well does crystal plasticity represents the mesoscale behavior of large populations of dislocations (as carriers of plastic strain)? The literature shows consistently that only moderate agreement is found between experiment and calculation. We supplement this with a current example of microstructure evolution in the interior of a copper sample subjected to tensile deformation. Non-destructive measurements of orientation fields were performed using the near-field high-energy X-ray diffraction microscopy (nf-HEDM) technique at the Advanced Photon Source (APS). A single two dimensional slice of microstructure containing $\sim$ 150 grains was tracked through multiple strain states, starting from highly ordered grains and tracking lattice rotations and defect accumulation up to 14% elongation. In accord with the literature, comparison with crystal plasticity models indicates reasonable qualitative agreement but significant variations between simulation and experiment are apparent at the scale of individual grains. The conclusion is that, in order to be able to quantify the effects of microstructure on the distributions of slip, orientation change and damage accumulation, the empirically derived constitutive relations used in continuum scale simulations need to be improved. Equally important will be the development of large scale simulations of polycrystals that directly model dislocations.

Keywords: nf-HEDM, Plastic deformation, Microstructure, Texture, Micromechanical modeling

1. Introduction

The deformation of crystalline materials continues to challenge our understanding of the behavior of large populations of defects, which in this case concerns dislocations as the line defects that carry plastic strain. The main objective of this article is to make the case that we are not in a good position to predict the deviations from mean values as plastic strain accumulates in polycrystalline materials because we do not have adequate models for the behavior of large populations of dislocations. This is important because plastic deformation is the precursor to damage initiation such as the formation of cracks and voids. Understanding the influence of microstructure on such processes depends on accurate calculation of fields in deformation so that extreme values are well characterized. Minimizing discrepancies between current models and experiments will lead to better diagnosis of in-service components as well as allow the possibility to design and manufacture next generation materials with advanced properties, such as high mechanical strength and ductility.

The properties and ways in which individual dislocations respond to mechanical loading are well understood [1], often in elegant detail. To take just one example from the enormous literature, Srolovitz *et al.* [2] have modeled the way in which individual dislocations bypass obstacles such as second phase particles during which they adopt strongly curved conformations that resemble a coiled rope. Recall that elastic strains in metals rarely exceed 0.001% and so a plastic strain of 10% is already comparatively large. To appreciate the numbers of dislocations involved, a typical crystallite or grain size is of order 10 μm and the dislocation density can reach 10^{+14} m^{-2} after 10% strain, which corresponds to roughly 10^5 dislocations threading through each grain. Perhaps

*Corresponding author.
Email address: reeju@lanl.gov (Reeju Pokharel)

because of the large numbers involved, there is ample evidence that plastic deformation is successfully modeled at the statistical level. Dislocations at low temperatures are constrained to move conservatively (with only local atomic rearrangements) with specific, crystallographic slip plane and slip direction, the combination of which we term a slip system. As described in more detail below this constrained motion results in lattice rotation towards preferred orientations [3]. The slip geometry has long been incorporated into simulations to successfully model the evolution of orientation distributions *aka* texture [4, 5]. However, as we shall show, comparisons of experiments and simulations at the scale of grains show limited agreement, and even that is achieved only in some average sense. The most likely culprit is the commonly used relationship between the shear stress on a slip system and the resulting slip rate (as the product of mobile dislocation density and drift velocity). The constitutive relation, Eq. **??** below, assumes a smooth, monotonic albeit highly non-linear relationship between resolved shear stress and slip rate, and has proven to be very useful for continuum-scale simulation. Nevertheless the simulations do not adequately reproduce local variations in orientation or strain. Although the equation is based on plausible analysis of the kinetics of dislocation motion [6], it has not been obtained from detailed studies of the behavior of large dislocation populations. It has been noted many times that dislocation motion occurs in a non-steady fashion, e.g. Kubin *et al.* [7]. Numerous results available in the literature clearly demonstrate the substantial challenges that still exist in developing models that are accurate physical descriptors of the observed phenomena.

1.1. Dislocation Storage

The lack of agreement manifests itself in various ways. When dislocations intersect with themselves in large numbers their behavior becomes less well defined and one can say that no analogue to statistical mechanics (of e.g. gases) has been worked out for large populations of dislocations. This absence of a statistically based non-equilibrium theory is an important limitation in our ability to describe the collective behavior of dislocations that governs almost all aspects of the mechanical properties of materials. Cottrell famously remarked 60 years ago that the increase in hardness that results from the tangling of dislocations on intersecting slip systems, i.e. work hardening, is a difficult problem for which no theory is likely to be available in the near future [8]. Another manifestation is the development of non-uniform densities during plastic deformation. After large strain and at high deformation temperatures, dislocations organize themselves into subgrains i.e. μm-sized regions with negligible dislocation density separated by thin walls of high density that are essentially low angle boundaries. At the other extreme dislocations may accumulate as blocks of a random forest separated by layers in which larger shear strain has occurred, known as shear bands. Under intermediate conditions, dislocations form cells (equiaxed or elongated) with low densities in the interiors versus high densities in the walls, see [9]. Considerable effort has been devoted to reproducing this range of dislocation microstructures using both continuum and more detailed dislocation dynamics simulations with very limited success [10]. To set against this, it is important to note recent efforts to develop requirements for constitutive relations based on dislocation theory such as [11]. Groma in particular makes analogies to plasma physics (in order to account for long range interactions) in developing a theory for dislocation density in 2D [12]. Although the mathematical descriptions are only valid for a fixed population of straight dislocations, numerical solutions with variable dislocation densities provide interesting and plausible non-uniform dislocation distributions similar to those observed for fatigue. Zaiser and Hochrainer [13] obtained stress-strain curves based on a continuum analysis albeit for deformation of a thin film, which they based on earlier developments by Groma. These examples point to a slow but steady development of a body of theory that may eventually provide the desired dislocation analogue to statistical mechanics. Taken as a whole, these issues also serve to illustrate the importance of mesoscale science in the sense of complex behavior that arises when large populations of defects are allowed to interact [14, 15]. Later in the article we describe the Voce equation, Eq. 3 below, that is commonly used as a constitutive description of work hardening but it is important to note that this is purely empirical and there is no such constitutive description that has been derived from dislocation theory directly.

1.2. Two Major Challenges

The major scientific challenges identified here are a) the need for a statistical mechanics of (large populations of) dislocations and b) the need for improved numerical techniques to enable simulations of dislocation flow in polycrystalline materials. The first of these challenges also needs to be translated into engineering terms in the sense that better constitutive relations are needed for use in continuum codes. For the latter challenge there are some tentative steps that have been taken to develop more generally capable discrete dislocation simulation methods, e.g. Lei *et al.* [16] who represent the dislocations as eigenstrain fields and use a phase field method to update the dislocation positions as a function of the forces on them. Boundary conditions can also significantly affect the fidelity of simulations. Even though some of the work

cited here paid careful attention to boundary conditions and even varied them in order determine the sensitivity of the results, the level of agreement was similar in all cases. Nevertheless, it is possible that further refinement of the treatment of boundary conditions will be required.

1.3. Outline

We first review the work that has been done to compare experimental measurements of strain and/or orientation change at appreciable plastic strains, i.e. those above $\sim 2\%$, with theoretical calculations using crystal plasticity. The intent of the calculations is to reproduce the experiments using rules for the flow of dislocations that have been homogenized to the level at which the geometry of slip determines the plastic response but individual defects are not included. The approach is summarized below. Limiting the discussion to cases with appreciable plastic strain ensures that the effects of elasticity can be neglected [3].

We complete the article with an example of a current investigation of this sort that considers uniaxial extension in copper with non-destructive scanning in a particular layer of the sample with high-energy x-rays [17]. The aim is to illustrate recent advances in this area with more detailed analysis of the development of orientation gradients. We describe the sample, experimental set-up, data collection and preprocessing procedures for nf-HEDM as applied to the in-situ tensile test. Information on orientation gradients and misorientation development is then extracted from the orientation maps measured at different strain levels. We compare experimental observations on lattice reorientation with results from the fast Fourier transform (FFT) based crystal plasticity model [18, 19, 20] and the Taylor model [21]. Finally we discuss some of the advantages and disadvantages of current measurements and point the way towards larger, fully three dimensional data sets that are becoming available.

2. Overview of Spatially Variable Plastic Response

We now motivate the paper by reviewing the importance of understanding the local variations in plastic deformation. The practical significance of such variations occurs via the formation of "hot spots" i.e. locally high values of stress or tractions on an interface where one might expect damage to initiate. Hot spots are much discussed in reference to energetic materials (explosives) as discussed by Field [23] and many others. Localization of plastic flow into shear bands has been noted as a source of local maxima in temperatures i.e. literal hot spots [24]. The significance of hot spots in deformation to the formation of fatigue cracks is also almost self-evident [25].

2.1. Weakest Microstructural Feature

A more specific aim of such comparisons follows from consideration of materials properties such as brittle fracture and fatigue, for which the statistics of extreme values have been successfully applied. The basic physical idea is to treat failure as revealing the weakest microstructural feature of the system. Starting with da Vinci's early efforts to quantify the strength of ropes [26], followed by Mariotte's more quantitative work [27], fracture became a popular application of extreme value statistics, e.g. Epstein [28], Freudenthal and Gumbel [29]. Describing the overall statistics of the results of mechanical testing does not, however, expose the underlying connection to materials microstructure, or the still more fundamental behavior of large populations of dislocations. Various authors have linked such extreme value statistics to various microstructural features such as nonmetallic inclusions in metals and small cracks or voids in ceramics, e.g. Murakami [30]. Przystupa *et al.* linked fatigue life in an aluminum alloy to extreme values of void size [31]. More recently, Przybyla *et al.* have published a series of papers seeking to connect specific microstructural features such as slip activity to fatigue life predictors such as the Fatemi-Socie parameter, grain size, and grain orientation [32]. Such efforts clearly represent a top-down approach to the problem.

2.2. Dislocation Modeling

Dislocations can be modeled as discrete defects where the atomic details are neglected. Dislocations are simulated as sets of line segments that obey predetermined rules about the connectivity of the segments (e.g. conservation of Burgers vector), forces between segments (Peach-Koehler force), interactions between dislocations (e.g. locks of various types, or cross-slip) and rates of motion. Such *dislocation dynamics* (DD) models allow large numbers of dislocations to move and interact in a given volume, which, however, is generally restricted to being a single crystal with a low index direction parallel to the loading axis [33]. Notwithstanding these limitations, DD simulations have proven useful for investigating many aspects of plastic deformation and, in particular, the relationship between the shear stress required to move dislocations across a slip plane through a "forest" of obstacles, which provides detailed information about *critical resolved shear stress*. Several authors have used DD models to address problems in cyclic loading and Deshpande *et al.*, for example, have used the technique to model fatigue crack growth under cyclic loading [34]. Brinckmann and van der Giessen used DD to identify localization of dislocation escape from a single crystal that could give rise to a large enough slip step to initiate a fatigue crack [35]. Even this effort could only look at the interior of an individual,

symmetrically oriented grain and could not incorporate the effects of microstructure as conventionally understood at the microstructure scale.

2.3. Microstructurally-resolved Plasticity

Previous work on microstructurally-resolved plasticity has addressed a number of issues similar to those examined here. Barbe et al. [36, 37] found that, whereas the global response is insensitive to mesh refinement, the amplitude of local variations in stress increases slowly with increasing mesh refinement. Diard *et al.* [38] performed finite element simulations on polycrystals with properties for hexagonal metals. Although they determined that more than 400 integration points were sufficient to resolve intragranular gradients in stress and strain, they did not arrive at any definite conclusions about the influence of grain boundaries. Kanit *et al.* [39] examined the differences arising from using a mesh conformed to the grain structure, i.e. with relatively smooth grain boundaries, versus a voxel-based mesh, i.e. with stair-stepped boundaries. They found only minor differences between the two cases in the local field values. They also noted that great care must be used in determining how large a volume may be regarded as representative, in the sense of demonstrating converged values for properties such as modulus. The dispersion in modulus of thermal conductivity converges significantly more slowly (with numbers of realizations) than the mean values, not surprisingly. There is a large literature that deals with various aspects of the "representative volume element" that is, however, out of scope for this review.

2.4. Correlations to microstructure

In general, the available results of microstructurally resolved simulations show that in single phase polycrystals, at least, substantial intragranular gradients in stress and strain exist although the grain structure is always apparent in the stress and strain fields. Lewis *et al.* [40] used anisotropic elasticity FEM for a 3D microstructure of a commercial stainless steel Al6XN, and investigated correlations of the hot spot (von Mises equivalent stress) distribution, distance to the nearest grain boundary, grain boundary character and imposed loading condition using various visualization and analytical techniques. No clear correlations were found although Rollett *et al.* found that both high and low stresses are found near grain boundaries [41]. The spatial distribution of hot spots and its relation to microstructural features vary by imposed loading conditions. Clearly there is an important, mesoscale need to demonstrate that close agreement can be obtained between polycrystal plasticity calculations and experiments at the scale of grains in order to be able to predict distributions of strain, stress, damage and other technologically important aspects of mechanical loading.

3. Brief Synopsis of Crystal Plasticity

Studies of metal deformation are generally carried out at a length scale that spans at least one grain if not many grains in a polycrystal. Setting aside nanostructured materials for the moment, the minimum grain size generally found in structural materials is about 1 μm. Since dislocation densities easily reach $10^{16} m^{-2}$ this means each grain can contain upwards of 10^4 dislocations. Thus current practice is to omit any direct representation of the dislocations (or twinning systems) that carry the strain and use constitutive relations that describe the geometry of slip. Empirical formulae are then required to compute the hardness associated with each slip system, the parameters of which are obtained by fitting to whatever experimental data is available.

3.1. Schmid law

When analyzing straining experiments, particularly for tensile test on single crystals, the simplest way to understand the anisotropy of slip is to compute Schmid factors. The Peach-Koehler force [1] codifies the fact that stress couples to a dislocation via the virtual work principle. For conservative motion of a dislocation, i.e. glide, this means that we project the stress, $\boldsymbol{\sigma}$, onto the slip direction $\mathbf{b}$ and slip plane normal $\mathbf{n}$ (as unit vectors) to obtain a resolved shear stress, τ^s.

$$\tau^s = \frac{1}{2}\left(\mathbf{b}^s \otimes \mathbf{n}^s + \mathbf{n}^s \otimes \mathbf{b}^s\right) : \boldsymbol{\sigma} = \mathbf{m}^s : \boldsymbol{\sigma}, \qquad (1)$$

where $\mathbf{m}^s$ is the Schmid tensor of slip system (s). Schmid's Law then states that slip occurs once τ^s reaches a critical value, the *critical resolved shear stress* (CRSS). This CRSS is that required to generate long-range motion of dislocations across their slip planes, as mentioned above. For a uniaxial stress state, i.e. one non-zero stress component parallel to an axis $\mathbf{t}$, it is easy to define a *Schmid factor, m* which is equal to $m = (\mathbf{b} \cdot \mathbf{t}) \times (\mathbf{t} \cdot \mathbf{n})$ (all unit vectors). The maximum value is $m = 0.5$. Slip is then expected to occur on the slip system with highest Schmid factor. Thus a "hard grain" is one that has a small value of the maximum Schmid factor; by contrast, a "soft grain" has a large Schmid factor. Note that this simple analysis is suitable only for single crystals under particular boundary conditions such as uniaxial tension.

3.2. Crystal Plasticity

Crystal Plasticity (CP) refers to a constitutive equation that is commonly used to describe the plastic response of metals to mechanical loading [42]. It

assumes that slip occurs by motion of dislocations on slip systems with crystallographically defined slip planes and slip directions. The slip direction corresponds to the Burgers vector. Taking fcc metals such as aluminum, nickel and copper as examples, the standard slip system is notated in Miller indices as $\{111\}\langle 110\rangle$, corresponding to close packed plane (normals) and close packed directions, respectively. Based on a great deal of experience with the kinetics of slip [6], the slip rate $\dot{\gamma}^s$ on a given slip system s is assumed to be proportional to the resolved shear stress τ^s normalized by a hardness or *(CRSS)* τ_c^s and raised to some power n:

$$\dot{\gamma}^s = \dot{\gamma}_0 \left(\frac{|\mathbf{m}^s : \boldsymbol{\sigma}|}{\tau_0^s} \right)^n \times \operatorname{sgn}(\mathbf{m}^s : \boldsymbol{\sigma}), \qquad (2)$$

where $\dot{\gamma}_0$ is the reference shear rate. It is important to note this constitutive relation is convenient to use because it removes the so-called ambiguity problem in the Taylor model whereby there are certain (tensor) stress states that can activate multiple slip systems in a given grain. In fcc crystals, however, these stress states activate eight or six slip systems simultaneously, which means that an arbitrary choice must be made of which combination of slips is to be used to satisfy the imposed strain, if the slipping rate is rate-insensitive i.e. a binary function of the resolved shear stress about the CRSS. By making the slip rate a smooth, continuous function of the resolved shear stress there is a unique relationship between the applied (tensor) strain rate and the corresponding set of slip rates [3]. Nothing in this approach, however, takes account of spatial or temporal variations in dislocation activity. It has proven to be very useful for modeling and predicting texture development in polycrystalline metals [43, 44].

3.3. Constitutive descriptions of strain hardening

As deformation accumulates, the evolution of the critical shear stress must be specified by a constitutive relation. At this point in time, none of the commonly used relations have been derived from dislocation theory, although certain efforts have come close e.g. [7, 45]. As an example of one of the commonly used empirical relationships, the extended Voce law [46] is written as

$$\tau_c^s = \tau_0^s + (\tau_1^s + \theta_1^s \Gamma)(1 - exp(-\Gamma|\theta_0^s/\tau_1^s|)) \qquad (3)$$

where Γ is the accumulated shear at any material point and τ_0, θ_0, θ_1, $(\tau_0 + \tau_1)$ are the initial critical resolved shear stress, initial hardening rate, asymptotic hardening rate, and back-extrapolated threshold stress, respectively. Finally, the change in critical stress in each slip system is given by

$$\triangle \tau_c^s = \frac{d\tau_c^s}{d\Gamma} \sum_{s'} h^{ss'} |\dot{\gamma}^{s'}|, \qquad (4)$$

where $h^{ss'}$ is the hardening matrix. In order to capture a correct lattice re-orientation, it is important to know the effects of s' slip systems on the activity of the slip system s. The hardening parameters are calibrated in the crystal plasticity models to predict the mechanical behaviors and properties of structural materials. Many variations on this basic approach are possible. Franciosi *et al.*, for example, showed that varying the critical resolved shear stress on each system is needed in order to reconcile the differences between tests on different orientations of single crystals with tests on polycrystals [47]. Furthermore, each slip system can harden other slip systems at varying rates depending on the geometry of slip (Burgers) vectors and intersections of slip planes; this phenomenon is known as *latent hardening*. The recent article by Roters *et al.* about crystal plasticity reviewed the current state of finite element modeling of materials that includes the physics of dislocation flow [48]. There are, of course, many other constitutive equations in use, all of which are empirical attempts to capture the effect of large populations of dislocations interacting with each other as well as with obstacles such as precipitates [49]. The nearest approach to obtaining the interaction parameters, h from dislocation theory is by Kubin *et al.* who analyzed the different strengths of dislocation junctions in fcc metals to obtain recommended values for the six different coefficients that remain after taking account of the various applicable symmetries [7]. They also took advantage of numerical simulations of dislocation dynamics to check for values of the mean free path of mobile dislocations. The result provided an empirical basis for the substantial variations in strain hardening rate observed when single crystals of different orientations are tested in tension.

3.4. Taylor factor, M

A simple scalar quantity that is useful in polycrystal plasticity is the Taylor factor, after the original analysis of large strain deformation of aluminum polycrystals [21] that related macroscopic behavior to dislocation slip on individual slip systems. The key assumption is that each grain in a polycrystal develops the same (tensor, deviatoric) strain as the average strain. It requires at least five independent systems to be active in each grain in order to accommodate an arbitrary applied strain. Because of this boundary condition, it is considered to provide an upper bound on the predicted macroscopic stress. The model enforces strain continuity across grains but stress equilibrium condition and neighbor interaction are ignored. The strain

rate in each grain is given by eq. 5 and the shear-rate for the active slip system is calculated from eq. 2. Finally, the hardening and grain orientation are incrementally updated at each strain step. Therefore, the Taylor model provides an easily calculable prediction of rotations based only on the geometry of slip in individual grains. It is known from previous work [50] to generally over predict rotations and to not capture the dispersion of rotation directions observed in local regions of the stereographic triangle. An outcome of the model is the Taylor factor, M, which is the quotient of the von Mises equivalent stress on the critical resolved shear stress for slip, or, equivalently the quotient of the sum of the microscopic slips on the von Mises equivalent strain. Thus a "hard grain" is one that requires a large macroscopic stress to obtain plastic deformation, or a large amount of microscopic slip in relation to the macroscopic strain increment; the converse statements are made in relation to "soft grains". Note that the choice of the von Mises equivalent quantities (as scalar measures of stress and strain) is somewhat arbitrary but commonly accepted. Methods for calculating the Taylor factor may be found in several texts, e.g. [3], and are generally based on the analysis of Bishop and Hill [51].

4. Full Field Crystal Plasticity Simulations

One of the variations of the polycrystal deformation models, inspired in a spectral formulation, was originally proposed by Moulinec and Suquet [52] to solve the micro-mechanical problem of linear elastic heterogeneous materials and later extended to non-linear two phase isotropic composites [53]. It was further combined with crystal plasticity (CP) by Lebensohn [18] to solve the micro-mechanical behavior of plastically-deforming polycrystals. The fast Fourier transform (FFT) based CP approach is an image based technique where the input microstructure is discretized into $N_1 \times N_2 \times N_3$ Fourier points and periodic boundary condition is applied, as required by the FFT algorithm. At each Fourier point, which coincides with a material point in the image, a constitutive equation, 5, is solved that gives a relation between the Cauchy stress and strain or strain-rate tensors. FFT-based methods have been developed for elastic, viscoplastic (VP) and elasto-viscoplastic (EVP) [54] constitutive behaviors to model full-field deformation in polycrystals. In this section, we will briefly describe the VPFFT approach, which we use in a comparison to experimental data in Sec. 7.

4.1. Viscoplastic FFT modeling

In the case of VPFFT formalism, the contribution of the elastic component is considered to be negligible and only the rigid viscoplastic regime of deformation is modeled. The deformation mechanism involves activation of slip or twinning modes, where the local constitutive relation that relates the plastic strain-rate $\dot{\boldsymbol{\epsilon}}(\mathbf{x})$ and deviatoric stress $\boldsymbol{\sigma'}(\mathbf{x})$ at each point $\mathbf{x}$ is given by

$$\dot{\boldsymbol{\epsilon}}(\mathbf{x}) = \dot{\gamma}_\circ \sum_{s=1}^{N} \mathbf{m}^s(\mathbf{x}) \left(\frac{\mathbf{m}^s(\mathbf{x}) : \boldsymbol{\sigma'}(\mathbf{x})}{\tau_c^s(\mathbf{x})} \right)^n \times \operatorname{sgn}\left(\mathbf{m}^s(\mathbf{x}) : \boldsymbol{\sigma}(\mathbf{x})\right), \quad (5)$$

where the sum is over all N active slip systems, where each individual slip rate is given by Eq. 2 and the evolution in the critical resolved shear stress is given by Eq. 3. The local stress tensor can be written as

$$\boldsymbol{\sigma}(\mathbf{x}) = \mathbf{L}^0((x)) : \dot{\boldsymbol{\epsilon}}(\mathbf{x}) + \boldsymbol{\phi}(\mathbf{x}) - \mathbf{I}_p(\mathbf{x}), \quad (6)$$

where $\boldsymbol{\phi}(\mathbf{x}) = \boldsymbol{\sigma'}(\mathbf{x}) - \mathbf{L}^0(\mathbf{x}) : \dot{\boldsymbol{\epsilon}}(\mathbf{x})$, is the polarization field. The VPFFT formalism utilizes Green's functions and FFTs, and consists of an iterative scheme based on the augmented Lagrangians (AL) [55] to efficiently calculate (in Fourier space and then by anti-transformation, in direct space) the local fluctuations in strain rate and the corresponding stress fields that fulfill the governing equations of strain compatibility and stress equilibrium, respectively, and the imposed boundary conditions for a periodic unit cell. Upon convergence, an equilibrated stress field constitutive relation with a compatible strain rate field, mapped onto a regular grid of Fourier points (where the local single crystal plasticity constitutive relation is known) are obtained.

4.2. Finite element modeling

An alternate to VPFFT is the finite element (FE) formulation, which is a continuum approach widely applied to predict polycrystal plasticity, where a single crystal constitutive equation is solved at each computational element point to model both small and large deformations. In the crystal plasticity FE framework, the local deformation gradient F_{ij} is multiplicatively decomposed as

$$F_{ij} = F^e_{ik} F^p_{kj}, \quad (7)$$

where F^e_{ik} and F^p_{kj} are elastic and plastic (deviatoric) components, respectively. To determine the state of each crystal in the polycrystal, the model calculates the Cauchy stress given by the Hooke's law in terms of Piola-Kirchoff stress S_{ij} as

$$\sigma_{ij} = \frac{1}{J} F^e_{ik} S_{kl} F^e_{lj}, \quad (8)$$

where $S_{ij} = C_{ijkl}(F^e_{ki}F^e_{kj} - \delta_{ij})$ and $J = det(F^e_{ij})$. In CPFEM, the rate of change of plastic deformation gradient L^p_{ij} is obtained as the sum of shear stresses $\dot{\gamma}^\alpha$

projected on each slip system α given by

$$L^p_{ij} = \dot{F}_{ik} F^{-p}_{kj} = \sum_{\alpha} \dot{\gamma}^{\alpha} \mathbf{b}^{\alpha} \otimes \mathbf{n}^{\alpha}, \tag{9}$$

where $\mathbf{b}$ and $\mathbf{n}$ are the slip direction and slip plane normal, respectively [55].

5. Experimental Probes

5.1. Surface characterization

There are two field quantities that are readily accessible on a surface. Strain mapping can be accomplished via tracking the displacements in either grids or spot patterns. Allais *et al.*, for example, showed that significant differences in strain accumulate in a two phase metal composite [56]. Kammers & Daly provide details of advances in the technique especially for use in the SEM [57]. For mapping crystal orientation fields, one of the most commonly used and widely available microstructural characterization techniques is Electron BackScatter Diffraction (EBSD). This is a versatile tool because it can be applied to essentially all crystalline materials whose grain size is no smaller than about 500 nm. EBSD has been invaluable in understanding local orientation gradients in deformed materials [58]. Recent developments have made it possible to perform in-situ deformation experiments, using EBSD [59]; however, it is important to bear in mind that it is a destructive technique that requires cross-sectioning and surface preparation and is mostly limited to post-mortem characterizations. Because the measurement is done at a surface, strain and other relaxations from bulk configurations must be considered.

5.2. 3D characterization

Defect accumulation and damage nucleation are local phenomena, and spatially resolved information on the crystallographic orientations is important in order to understand the internal response of the microstructure in accommodating external loads [60]. The advances in high-energy synchrotron based techniques allow non-destructive measurements of crystallographic parameters for microstructural characterizations. For example, high-energy three-dimensional X-ray diffraction (3DXRD) method developed by Risø group [61, 62, 63] probes bulk samples and provides information on the crystallographic orientation and elastic strain tensor averaged over a volume, commonly a grain. While 3DXRD measurements afford information about the center of mass of the diffracting volume, the drawback is that we are not able to obtain commonly expected data that resolve intragranular orientation gradients, which is considered standard for EBSD maps. Similarly, diffraction contrast tomography (DCT) is another variant of the non-destructive grain mapping technique that provides both the crystallographic orientation as well as the grain shape information, however, this technique is only limited to undeformed samples [64].

Developments in non-destructive materials characterization methods have been successfully employed to study microstructural evolution under thermo-mechanical loading conditions [65, 66, 67, 17, 50, 68], thus allowing better understanding of the heterogeneous materials behavior. In particular, the near-field high-energy X-ray diffraction microscopy (nf-HEDM) [69, 70, 71] is one of the synchrotron-based techniques that permits measurement of the spatially resolved orientations of grains that are embedded deeply in the bulk sample. This eliminates any concerns about surface relaxation effects, for example [72, 73, 17].

6. Review of Comparisons of Computation and Experiment

Comparisons of deformed microstructures with numerical simulations have been reported from time to time in the literature. There is also a substantial literature on strain measurement resolved to the scale of individual grains e.g. [74, 75, 76] but space does not permit us to include in this review.

6.1. Orientation mapping of individual grains

One of the earlier reports is due to Becker and Panchandeeswaran [77] who measured 32 individual grain orientations on the internal surface of a sample of nominally unalloyed aluminum with 0.15% Fe and 0.07% Si (by weight) using back scatter electron diffraction. Here the impurities served to limit the grain size while not substantially affecting the stress-strain behavior. This represented an early application of automated orientation mapping [22], permitted the initial, undeformed microstructure of the internal surface(s) to be mapped out and used as input for numerical simulation of the evolution under plastic straining. The sample was cut in two in order to be able to reassemble it after characterizing an internal surface and then compressing it at 375°C in a channel die to a 40% reduction in thickness. In this particular experiment, the sample was found to have undergone macroscopic shear in addition to the anticipated plane strain compression. Comparison of the orientations of the deformed individual grains with either the Taylor model or a more detailed finite element model showed good agreement for only a fraction of the grains. Some individual grains exhibited substantial differences with the calculations.

Panchandeeswaran *et al.* [78] extended the above study with more detailed orientation mapping and x-ray pole figure measurement; strain maps were not

measured. A finite element mesh was fitted to the initial structure as before and crystal plasticity was used to simulate the evolution under plastic strain. Comparison of the measured and predicted orientation distributions showed good agreement between the experimental and numerical simulation results. When a comparison was made at the scale of individual grains, however, the agreement remained poor. The (mosaic) spread of orientation within individual grains was substantial; one grain exhibited a spread of 25°, for example. Also, the orientation change of an individual grain was often substantially different in magnitude or even different in direction from that predicted by the simulation.

6.2. Tensile Tests

Lineau *et al.* [79] measured strain, via surface gridding, and orientation changes for a tensile test on an aluminum-killed mild steel. The strain map for the component parallel to the tensile axis exhibited significant variations in magnitude. They compared the orientation changes of 76 grains with Taylor model calculations in a self-consistent formulation although the details of the latter were not specified. The result was moderate agreement: some individual grains showed good agreement but others did not. No attempt was made to analyze the effect of neighbor grains on any given grain for the simple reason that a self-consistent Taylor model only contains interaction with an averaged (*a.k.a.* homogeneous) medium but no specific neighbor information.

Delaire *et al.* [80] made an oligocrystal of copper that had eleven millimeter sized grains and an approximately columnar structure. This permitted the use of a finite element mesh with only two elements through the thickness. The constitutive model used standard crystal plasticity with hardening parameters designed to match the observed stress-strain behavior. Tensile stretching was applied to the sample and the strain fields were measured at 7.5% and 33% von Mises equivalent strain. Comparison of the axial strain fields between experiment and simulation showed broad agreement, mainly because a few grains at one end had high Schmid factors that concentrated the deformation. Significant differences were, however, evident for both strain levels. Reasonable agreement between the measured and simulated orientations in terms of comparison on a pole figure at 7.5% were obtained but no comparison was reported for the larger strain.

Hoc and Rey performed a tensile test on a polycrystalline mild steel sample and measured the surface strain, for the component parallel to the tensile axis, for an area containing 114 grains [81]. As in other such tests, significant variations in strain were observed and the pattern suggested specimen-scale banding, which they termed mesobands. They ascribed the occurrence of these bands to the multiple combinations of dislocation slip that are possible in cubic metals. Without mentioning how the orientations were measured (but presumably with EBSD or channeling patterns), they used crystal plasticity FEM to simulate the test. They claimed to observe agreement between the simulated and measured strain maps but the degree of agreement was equally as poor as for the other comparisons reported here. One additional point that they made was that embedding the measured set of grains inside the surrounding medium resulted in weaker strain gradients than for the experimental case where the measured grains were at a free surface. This was, however, the only discussion of boundary conditions, in contrast to more recent works. Tatschl and Kolednik [82] performed a similar experiment but used a miniature tensile stage in an EBSD-equipped SEM to characterize a high purity copper sample with a relatively coarse 100 micron grain size. They performed a detailed analysis of both the strain fields and the reorientation of the crystal lattice. They compared their experimental lattice reorientations with calculations based on the Taylor model and found that only certain areas showed good agreement whereas some did not. The strain maps were notable for the marked variations in magnitude of each component and the concentration of strain at certain grain boundaries. In this, a full field calculation of the deformation was not attempted. Cheong and Busso used a full field crystal plasticity (finite element) simulation to analyze a similar tensile test on an oligocrystal of Al 0.5%Mg paying particular attention to the shear banding present in the measured strain map [83]. Again, even taking into account crystal plasticity, only moderate agreement was achieved.

Zhao *et al.* made an oliogcrystal of aluminum with a columnar grain structure via high temperature annealing [84]. The top and bottom surfaces were orientation mapped and also gridded for strain measurement. The sample had dimensions of 21 mm (long), 8 mm (wide) and 1 mm (thick) and contained 22 grains. The texture was dominated by a ⟨100⟩ fiber, meaning that each grain had a ⟨100⟩ axis close to the normal of the observation plane. The axial strain fields were measured at several strain steps up to a maximum of about 11% and exhibited minor differences in accord with the small variations in grain boundary position. A crystal plasticity finite element model with hardening parameters derived in part from the work of Franciosi *et al.* [47]. was used to simulate the experiment. As with the other reports cited here, the axial strain fields showed broad agreement, mainly because grain number six was sufficiently compared to all the others that the strain concentrated in that particular grain. More detailed comparison shows significant differences, however, as did comparison of the

surface roughening profile.

Lebensohn *et al.* [19] analyzed EBSD maps of a copper sample tested in tension to about 11% strain. They took the map of the initial undeformed structure and generated a quasi-3D microstructure which they then used as input to a simulation using the VPFFT method, see 4 for a description. Reasonable agreement was found for the average re-orientation of the lattice in each grain. Orientation (mosaic) spread was also analyzed and the average disorientation was found to scale with grain size, which was also found in the simulation. There was also a trend with orientation such that the largest orientation spreads occur near the ⟨110⟩ corner of the unit triangle. Buchheit *et al.* [85] performed an experiment also on a copper polycrystal and compared it to a crystal plasticity finite element simulation. One comparison of particular interest here was that they examined the variation in orientation across a few grains and found only moderate agreement between experiment and simulation. The examination of orientation spread is a topic that we shall return to in later sections.

Rehrl *et al.* started with a coarse-grained austenitic stainless steel to obtain a bicrystalline tensile sample with cross section 1 x 1 mm [86]. They characterized both the strain and the orientation development at a strain of 28% and performed crystal plasticity finite element simulations using Abaqus and a strain hardening model due to Bassani and Wu [87, 88]. Although the CPFEM model showed good overall agreement with the experimental results in terms of both strain and orientation change, they highlighted a notable difference in terms of fragmentation of grains on a length scale of order 200 microns. This fragmentation took the form of banding in the "harder" grain that had smaller Schmid factors. By imposing, somewhat arbitrarily, a similar spatial variation in which slip systems were allowed to operate, the simulation could be made to reproduce the observed banding. The authors postulated that modifications might be possible to the crystal plasticity model to allow this to happen automatically in the simulations but did not propose any specific approach to the problem.

Choi *et al.* used a micro-tensile experiment with a pure nickel sample to measure strain variations [89]. The sample had dimensions 21 x 38 x 80 microns (width x depth x length) and a grain size of order 15 microns, such that there were only one or two grains across the width of the sample. 2.4% axial strain was imposed and then the entire gauge section was subjected to serial sectioning with EBSD leading to a reconstructed 3D volume, which in turn was used as input to CPFEM. Based on a grid of marker points, the strain was also mapped as a function of position. The mecanical response was calculated with several different assumptions about the boundary conditions and compared with the experiments both in terms of the strain maps and the local orientation gradients quantified in terms of a kernel averaged misorientation (KAM). In general terms, the strain map comparison showed reasonable agreement and yet there was more agreement between the different boundary conditions than there was with the experimental result. The same was found for the comparison of the orientation gradient maps.

6.3. Channel Die Tests

Raabe *et al.* [90] used strain mapping on the surface of a 15 x 10 mm sample of pure aluminum with 18 grains in view. In a sample subjected to 8% von Mises equivalent plane strain compression overall, some grains were measured to have twice that strain whereas others exhibited negligible accumulated strain. They used a conformal finite element mesh with about 6000 elements shaped to match the grain boundaries. In order to measure the importance of crystallographic slip, simulations were made with a purely continuum constitutive model as well as with rate-sensitive crystal plasticity as the model. This contrast showed that crystal plasticity introduces an important anisotropy. In addition, variations in the friction coefficient boundary condition minor differences in the pattern of strain over the region of interest. However, the similarities between the various crystal plasticity simulations were more obvious than in the comparison with the experimental strain map. More specifically, significant differences were observed on a grain-to-grain basis between experiment and simulation. Lattice reorientation was not considered in this work because of the small strain. Strong gradients in slip activity were noted in the vicinity of most grain boundaries, which will turn out to be significant elsewhere in this article.

Zaefferer *et al.* performed channel die compression tests on Al bicrystals of aluminum [91] with symmetric ⟨112⟩ tilt boundaries and misorientations of 8.7° (small angle), 15.4° (transition), and 31.5° (large angle). Thanks to the simple microstructure, a finite element model could be easily constructed for comparison with the experiments. Compression to a maximum of 50% reduction in thickness was applied in a channel die. The orientations were such that macroscopic shear strains resulted from the applied compression; similar shears were observed in the finite element simulations and the overall shape change was modeled well. Moreover the pattern of heterogeneous straining was reasonably well modeled, albeit with significant local variations. As in essentially all cases, a standard crystal plasticity model was used although latent hardening was applied. Lattice orientations were measured before and after deformation. Starting from the well annealed single orientations in each crystal, rotation occurred as well as

dispersion. Comparing the simulations to the experiments showed larger lattice rotations in the former and smaller dispersion, just as observed by Panchandeeswaran *et al.* [78]. The intermediate misorientation bicrystal (15.4°) showed larger orientation gradients in the vicinity of the boundary than the smallest misorientation. Shear bands in the largest misorientation bicrystal prevented such an analysis.

Ma *et al.* followed up on the previous work on bicrystals with symmetric ⟨112⟩ tilt boundaries with the same set of three different misorientation angles but deforming in simple shear instead of plane strain compression in order to avoid the problems associated with friction conditions, which are hard to quantify [92]. They also simulated the experiments with finite elements but used a modified crystal plasticity model. The modification [93] introduced a non-local hardening model for individual slip system according to separation into statistically stored ("SSD") and geometrically necessary dislocations ("GND"). This permits accumulated orientation gradients (from local variations in lattice rotation) to influence the hardness. In the case of simulations of the bicrystal shear experiments, an additional hardness was introduced for the grain boundary by including a layer of elements with higher flow resistance than for elements corresponding to bulk material. The simulations were also performed with a conventional crystal plasticity model that was termed "local hardening" in the sense that orientation gradients were not included in the hardening model. The comparison between the two sets of simulations and the experiments showed that the more complex model yielded substantially better agreement with experiment, both with respect to strain distribution and with respect to local variations in lattice rotation. The standard crystal plasticity model, for example, exhibited too-large lattice rotations and much larger dispersion than observed in experiment, whereas the non-local model showed good agreement.

Quey *et al.* deformed a split sample in a similar experiment to those reported by Panchanadeeswaran [94, 78] and studied grain fragmentation, which is the tendency of the lattices of individual grains to rotate in different directions as plastic strain accumulates. They also ran 3D crystal plasticity finite element simulations of the same 176 grains that were observed experimentally and measured fragmentation, i.e. the development of a grain boundary inside a grain with a misorientation greater than 15°. They found good agreement in the sense that fragmentation occurs most often for orientations where the lattice reorientation diverges strongly for small variations in initial orientation across a symmetry line. However, a larger fraction of grains fragmented in the simulations than in the experiments, which was ascribed to the experimental observations being limited to the sample surface, as opposed to the 3D simulations. Simulations are known, however, to result in larger lattice rotations (and sharper textures) than observed in experiments, which may provide an alternate explanation of the discrepancy.

6.4. Other Tests

Wang *et al.* examined slip behavior under four-point bending in a polycrystalline commercial purity Ti [95]. In this experiment, EBSD was used to map the area of interest before deformation and synchrotron x-ray radiation was used to map orientations using the DAXM technique afterwards [96]. The advantage of the DAXM technique is that the Laue figures that are collected can be analyzed for streaking of the diffraction spots such that dislocation activity can be inferred. The objective of using four-point bending was to concentrate the tensile strain on the observable surface since the DAXM technique is limited to near-surface measurement. Comparison of the experimental observations with crystal plasticity finite element simulations showed only moderate agreement both for slip system activities and for lattice rotations. Since Ti is hexagonal, the plastic anisotropy is stronger than for cubic metals. The grain size was of order 50 μm which was large enough that the DAXM could not map the grain structure in three dimensions. Yang *et al.* performed a follow-up experiment on the same materials also with four-point bending and measured surface height variations over a 14-grain patch area. Once again, comparison of activity levels of the various slip and twinning systems was satisfactory at the scale of individual grains but the spatial variations were not well captured by the simulations.

Sarma and Dawson used CPFEM to investigate the variation in deformation from grain to grain in a polycrystal [97]. They used a mesh with, in effect, one grain per quadrilateral element, with the rate-sensitive formulation described above. They determined that each component of the (deviatoric) strain rate conforms to a normal distribution. They tested the commonly held view (in materials science) that the local value of the strain rate should anti-correlate with the Taylor factor; such a correlation exists but is weak compared to width of each Gaussian. Their conclusion was that grains are strongly affected by their neighbors. In related work, Lienert *et al.* measured elastic strains grain by grain in a copper polycrystal [98] using a so-called far field diffraction experiment on a high energy beamline at the Advanced Photon Source. They selected grains with a ⟨110⟩ axis parallel to the loading axis and also ran polycrystal simulations with anisotropic elasticity. They found variations about the mean strain of order 6%, with fair agreement with the simulations, which they considered acceptable because the full 3D microstructure could not be measured. Since the orientation of the probed grains with respect to the loading axis was

fixed, these variations could only come from neighbor interactions. Although this addressed elastic strains, resolved shear stresses on slip systems are determined by the local elastic strains, so this provided an experimental verification of the variability caused by such neighborhood effects. Miller *et al.* extended this approach to measuring elastic strains for the four low order planes using synchrotron high energy x-rays [99]. Strain Pole Figures (SPFs) were derived from this diffraction data, which in turn led to distributions of elastic (tensor) stress over orientation space. Representative 3D polycrystal microstructures and elasto-plastic finite element modeling were used to obtain the same stress distributions, before and just after plastic yield. Comparisons of experimental and theoretical results show, as for the earlier work, good but far from perfect agreement.

7. Example: Near-field HEDM observation of plastic deformation in bulk polycrystalline Copper

In the following, we describe the evolution of internal microstructure during in-situ tensile loading of a Copper sample. A single two dimensional cross-section is tracked through a series of macroscopic strain states. We characterize lattice rotations and the development of intra-granular orientation variations and make direct comparisons to the VPFFT model. The purpose is to emphasize the key role that can be played in model validation by recently developed high energy x-ray capabilities that probe internal microstructures in a non-destructive manner. Fully three dimensional characterizations will follow. A prior proof of principle measurement was carried out by Li *et al.* [17]. In the current work, a larger sample cross-section is used, where we begin the measurement with an undeformed microstructure and use small, incremental strain steps so as to more fully characterize the onset of deformation. The experimental apparatus for near-field HEDM compatible tensile strain measurement was developed by Lind *et al.* and was used in a similar study of plastic responses in Zirconium [100].

7.1. Material & methods

7.1.1. Material: Pure Copper

The specimen is 99.995% pure, oxygen free electronic (OFE) copper and this and all relevant details are given in [101]. The sample was machined from a half hard rolled plate (equivalent to a rolling reduction of $\sim$ 21%). The cylindrical sample was machined to have a 1 mm diameter, 1 mm long cylindrical gauge section with the tensile axis parallel to the cylinder axis. A heat treatment protocol was developed through multiple steps of polishing, etching, and annealing, coupled with EBSD characterization of test coupons. The initial state of the nf-HEDM sample was obtained by annealing (after machining) in a forming gas (95% N_2, 5% H_2) environment at 550° C for an hour. This resulted in well ordered grains with an average size of $\sim 60\ \mu$m.

7.1.2. Experimental methods

Measurements were performed at beam line 1-ID of the Advanced Photon Source (APS) at Argonne National Laboratory. The essentials of the beam line hardware and experimental protocols are given in [69, 102] In the current measurement, we use E = 64.3 keV photons which have an absorption length in copper of just over one millimeter which roughly matches the sample cross-section dimension. The beam is focused in the vertical direction to $\approx 3\ \mu$m while the width is 1.3 millimeters. This beam illuminates a quasi-planar cross-section of the sample as it rotates on a high precision air bearing stage. Detector images are obtained as the sample rotates through $\delta\omega = 1^\circ$ intervals over a 180° range. The detector system has $1.5 \times 1.5\ \mu\text{m}^2$ pixels with a field of view of 3×3 mm.

7.1.3. Load system

A custom-designed miniature loading system was used in order to be able to develop plastic strain in the specimen while positioned in front of the x-ray beam [101]. The cylindrical geometry near the sample gauge section, without any force bearing posts as in standard load frames, allows the near-field detector to approach within a few millimeters of the sample even during the 180° rotation required for data collection. [103] For this measurement, rotation axis-to-detector distances, $L = 5.8, 7.8,$ and 9.9 mm were used; the $L = 9.9$ mm distance was used only for a few measurements so as to allow robust optimization of the experimental geometry by the microstructure reconstruction code. [71]

In order to probe approximately the same cross-section of the sample as it was loaded, the entire sample stage was translated upward by one-third of the applied displacement of the strain stepping motor. As shown below, this resulted in the illumination of a common set of grains in each strain state. Data were collected in twelve strains states spanning from essentially no deformation up to 14% tensile deformation. Macroscopic strain and strain states are summarized in Table 2. The macroscopic stress-strain curve was checked to be similar to previous reports for electrical-grade, highly pure copper [104].

7.1.4. Computational reconstruction of microstructure

The forward modeling method (FMM), as described in [69, 71], is used to reconstruct the orientation field by matching simulated diffraction to the

experimental data. The spatial resolution of the reconstructions presented here is determined by the use of a mesh of equilateral triangular voxels (volume elements) with side-lengths of 2.8 μm. For each voxel, 80-150 simulated diffraction peaks are compared to the experimental data; this range in number is due to variations with orientation and with voxel position in the number of peaks that strike the detector. The orientation resolution in well annealed material is $\approx 0.1^\circ$ [105] and with increasing strain, the resolution decreases to $\approx 0.5^\circ$ [17]. The reconstruction algorithm can fail to find a solution near grain boundaries. The accumulation of plastic strain results in smearing of spots because of the well-known fragmentation of grains. This results in overlap of low order diffraction peaks as well as a drop in intensity of higher order Bragg peaks. Both effects tend to degrade the quality of the orientation reconstruction but, fortunately, the quality of the indexing from the FMM degrades gradually rather than failing abruptly [71]. Use of improved signal extraction from the raw detector images significantly improves reconstructions of deformed states relative to previous work [103, 100] and allows us to reconstruct even at the 14% level of strain. A "confidence" parameter, C, is reported for each reconstructed voxel. C is defined as the fraction of simulated Bragg peaks that strike detectors (using the optimized crystal orientation) that overlap experimentally observed diffracted beams. Since all simulations, from fully ordered to highly deformed states, extend to the same high order scattering, we find that C decreases steadily with increasing plastic strain [66, 71, 106]. More complete analysis of the improvements in the FMM method for plastically strained materials will be described in future publications.

7.2. Experimental results

7.2.1. Analysis details

In order to avoid surface effects, analysis presented here is restricted to material inside a radius of 0.4 mm whereas the sample radius is 0.5 mm. From the orientation maps in Fig. 1, it is evident that most of the same grains remain in the sampled cross-section as the sample is extended in tension by pulling along the normal to these images. There is, however, some unavoidable variation resulting from the approximate tracking procedure described above and the flow of material between states. Hence, small grains present in one of the maps may be absent in others. We estimate that the illuminated section varied in position (relative to the original material point) by no more than four microns, as compared to (an unstretched) grain size of $\sim$ 60 μm. Importantly, a set of large grains remain in the orientation maps for each of the twelve strain states.

The maps of C in Fig. 1 show the expected overall behavior with strain. In the well ordered state of Fig. 1(d), C is reduced near grain boundaries because of detector discretization noise and background subtraction/peak extraction statistical noise associated with edges of diffraction spots [71]. In higher strain states, there is a growing area over which C is significantly reduced. However, there is considerable heterogeneity in this reduction implying that some grains remain well ordered even up to 14% strain.

7.3. Grain-scale Analysis

The 100 largest grains identified in pre- and post-deformation states are used to study the microstructure evolution and the development of orientation gradients as a function of external load. We use a registration procedure based on these grains to maximize the match between strain states. The process described by Lebensohn *et al.* [19] and by Li *et al.* [17] minimizes the average misorientation angle between two overlayed images. Due to the in-situ nature of the measurement, only a tilt of the sample would need to be adjusted and, in all cases, the tilt angle was assumed to be small and not considered in the registration algorithm.

7.3.1. Lattice orientation dependent rotation and orientation spreading

Grains can be tracked between strain states because the orientational disorder within them is relatively small compared to typical high angle grain boundary discontinuities in orientation. Voxels (reconstructed mesh elements) that comprise a grain are determined using a connected component analysis with some threshold misorientation angle, θ_{max}, as the criterion for determining boundaries. Here, we use $\theta_{max} = 5^\circ$ since this yields reasonably consistent collections of voxels across strain states. Grain averaged orientations, $\langle \mathbf{g} \rangle$, are then computed according to the procedures described in [107].

7.3.2. Lattice re-orientation

Fig. 2a shows the rotation of crystal lattices in individual grains which is caused by slip response to the tensile force combined with the spatial constraints of neighboring material. Large rotation angles are apparent near the $\langle 101 \rangle$ – $\langle 111 \rangle$ line with rotations tending to align a $\langle 111 \rangle$ direction with the tensile axis. Grains near the left end of the triangle exhibit smaller rotations with a weak tendency towards alignment with $\langle 001 \rangle$ direction and with perhaps a larger dispersion in rotation directions. The expectation from the Taylor model [21] is that tensile deformation should cause texture development with either $\langle 111 \rangle$ or $\langle 001 \rangle$ aligning with the tensile axis and this is seen in macroscopic measurements of cubic metals.

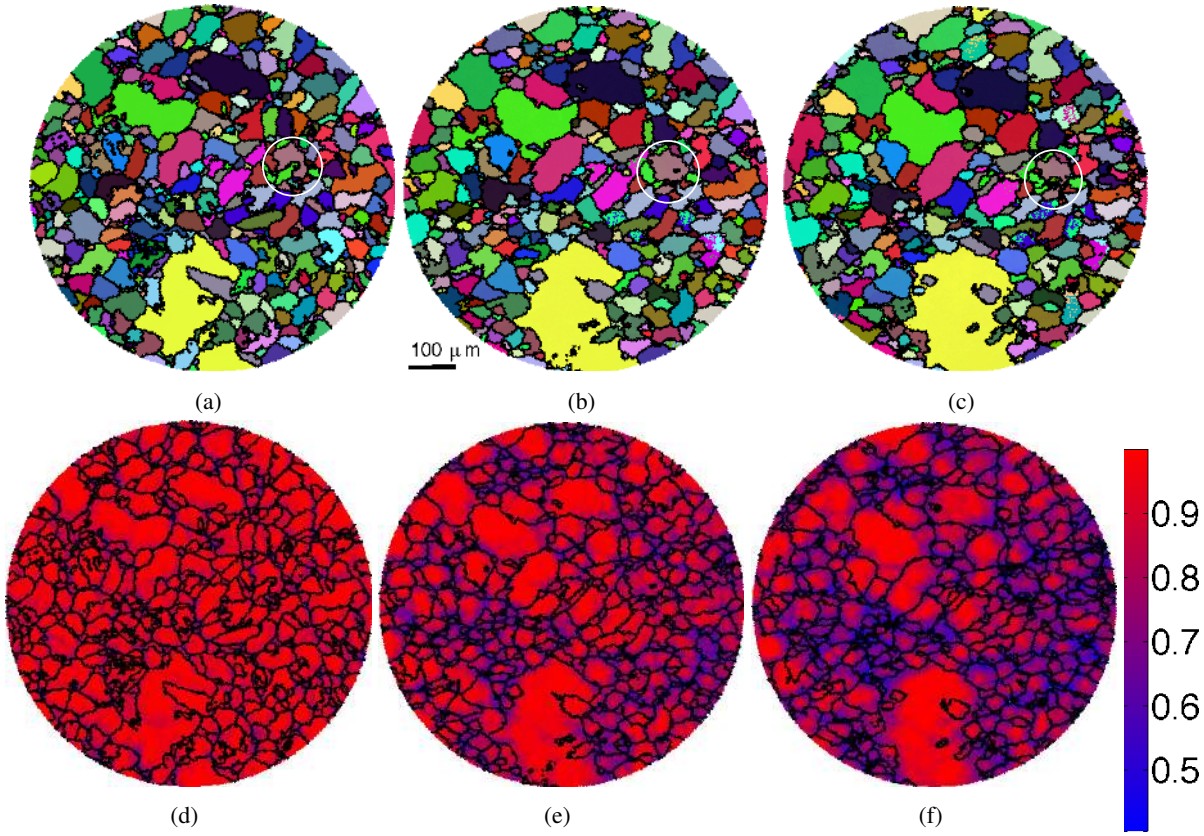

Figure 1: Reconstructions of internal microstructure in three strain states. All maps are truncated to 0.4 mm radii. Crystallographic orientations are shown at (a) 0.06%, (b) 7%, and (c) 14% strains. Colors are mapped from Rodrigues-Frank orientation components to the RGB color space. The large yellow grain (grain #2) in the bottom and the grain enclosed in a circle (grain #15) will be discussed in more detail in later sections. The corresponding confidence parameters, C, are mapped in (d) through (f). $C = 1$ indicates that all simulated scattering strikes experimentally observed intensity. In all the maps, black lines are drawn between pairs of voxels with misorientation angles greater than 5°; even in the most deformed state, these lines appear almost exclusively along grain boundaries.

The observations are consistent with previous work [108] that divides the unit triangle up into four main areas. Winther *et al.* noted a trend for rotation towards the ⟨111⟩ corner of grains close to the 111-110 edge, rotation towards the 111-001 line of grains near ⟨110⟩, rotation towards ⟨111⟩ of grains close to the the 111-001 line, and considerable variation superimposed on a general rotation towards ⟨001⟩ for grains close to ⟨001⟩. These observations are also consistent with recent work by Oddershede *et al.* [68].

7.3.3. Grain fragmentation

Fig. 2b shows a voxel-by-voxel image which demonstrates the dispersion of both rotation angles and directions within individual grains. In the initial state (blue), voxels are tightly clustered with $\approx 0.1°$ dispersion. Thus, initial grains are ordered to better than the measurement resolution used here. With increased strain, voxels corresponding to a grain become scattered but consistent trends in successive states are observed in that rotations tend to continue in a given direction(s). The distribution of orientations within a grain corresponds to the mosaic spread observed in the diffraction images. Interestingly, the nature of the orientation dispersion falls into at least two classes: simple broadening (shown in the expanded view of grain 2 and bifurcation, indicating grain fragmentation, as shown in the expanded view of grain 15. In the latter case, looking at only the rotation of the grain average orientation may be misleading. Further, in most cases, the dispersion in rotation angle is of the same order as the average angle. The FMM reconstruction also gives spatial information about the mosaic distribution as discussed further below.

The observation that averaged as well as local rotations in similar regions of the stereographic triangle vary in magnitude and direction implies that variables other than the tensile axis orientation are important. First, the tensile axis orientation does not fully specify the crystal orientation or the resolved shear stresses

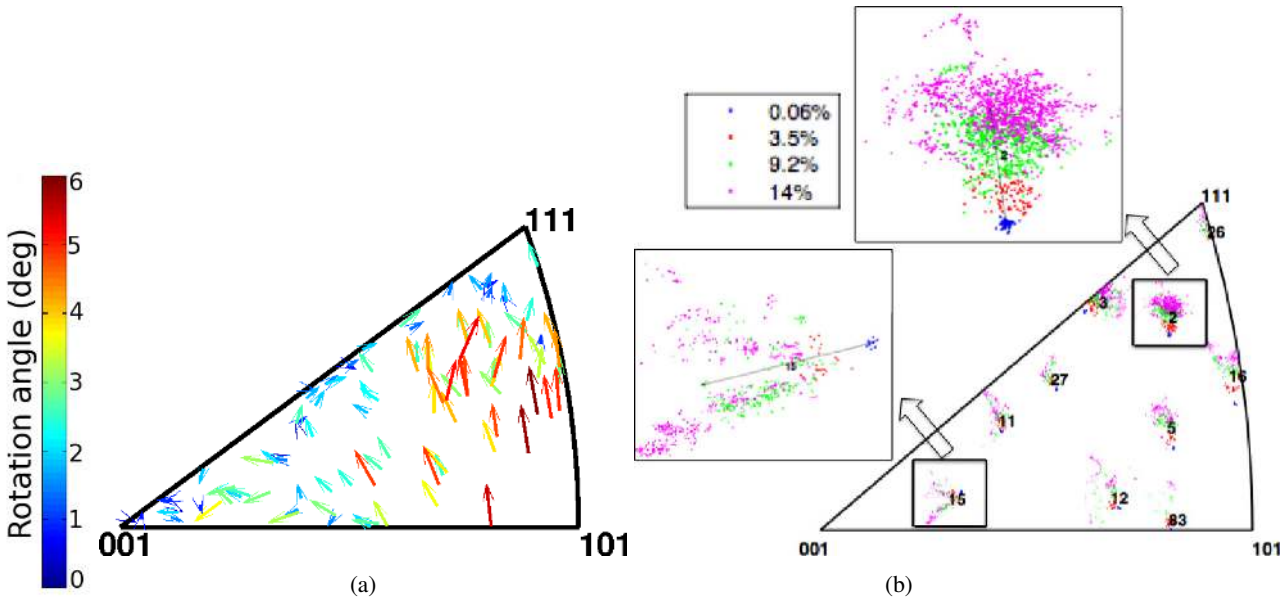

Figure 2: Inverse pole figures showing the location of the tensile axis in local crystal coordinates (reduced by symmetry to a single stereographic zone). (a) Grain cross-section averaged positions of the 100 largest grains with arrows pointing from the location prior to deformation to that at 14% strain. Colors indicate the averaged rotation angle. (b) Voxel based rotations. Points are shown for each reconstructed voxel making up 16 of the 100 grains. Colors here represent different strain states. Expanded views are shown for two grains exhibiting distinct behaviors that are discussed further below; straight lines indicate the grain averaged rotation.

on various slip planes. For this, one needs to know the rotation angle, say, ψ, around the specified tension axis. Recent work by Quey *et al.* [94], described in Sec. 6.3, tracks complete rotations in Rodrigues space and identifies systematic behaviors, specifically, dispersion versus bifurcation, depending on the degree of symmetry in the starting orientations. This appears to be an important and fruitful analysis route with which variations in local regions of Fig. 2a may be understood. In this experiment, however, fragmentation is observed for orientations that are not close to a symmetry line, as suggested by Quey *et al.* [94]. Within a well ordered grain, of course, ψ is essentially constant, so explanation of the behaviors seen in Fig. 2b presumably require specification of local neighborhood effects which perturb the local stresses experienced by grains. As noted above in Sec. 6.4, it is clear that local principal stresses deviate significantly in magnitude and orientation from those imposed macroscopically [65, 50, 98, 102, 109, 110]. These effects represent a challenge to modeling efforts [19, 54, 94, 97, 98, 99, 111] but need to be reproduced in order to describe meso-scale responses.

7.3.4. Spatial resolution of lattice rotation and defect accumulation

To characterize local lattice orientation disorder within grains, we compute two quantities: an intragranular misorientation, **IGM**, and a kernel averaged misorientation, KAM. **IGM** is computed for each voxel, i, by computing the misorientation, $\mathbf{IGM}_i = \Delta\mathbf{g}_i = \mathbf{g}_i\langle\mathbf{g}\rangle^{-1}$, between the local orientation and the grain average. A grain averaged value, $\langle\mathbf{IGM}\rangle$ or more meaningfully just the misorientation angle $\langle$IGM$\rangle$, can then be computed for each grain as a characterization of the scale of orientation variations within a grain. Color maps of **IGM** similar to the orientation maps in Fig. 1, or the scalar angle IGM, help to visualize sub-grain regions that are rotated relative to the rest of the grain. The quantity KAM for a voxel is computed as a mean misorientation angle with nearest neighbor voxels. In contrast to IGM, KAM is a local measure of orientation variation on the length scale of the reconstructed voxels. It is important to recognize that the voxelized orientation field is not a continuum quantity and care must be exercised in computing derivatives. In fact, specifically in the case of copper, it is well known that sub-micron sized dislocation cells can be expected at higher strain levels [112] and the HEDM measurement is not sensitive to such variations within reconstructed voxels. Further, the orientation that is assigned by the reconstruction of a voxel *is not* any sort of averaged value but rather is the orientation that is best represented in the diffraction images. For example, if the region spanned by a voxel contains cell wall material and an ordered cell, the latter will generate well defined diffraction whereas the wall material has a high dislocation density and therefore would generate a more diffuse pattern that may

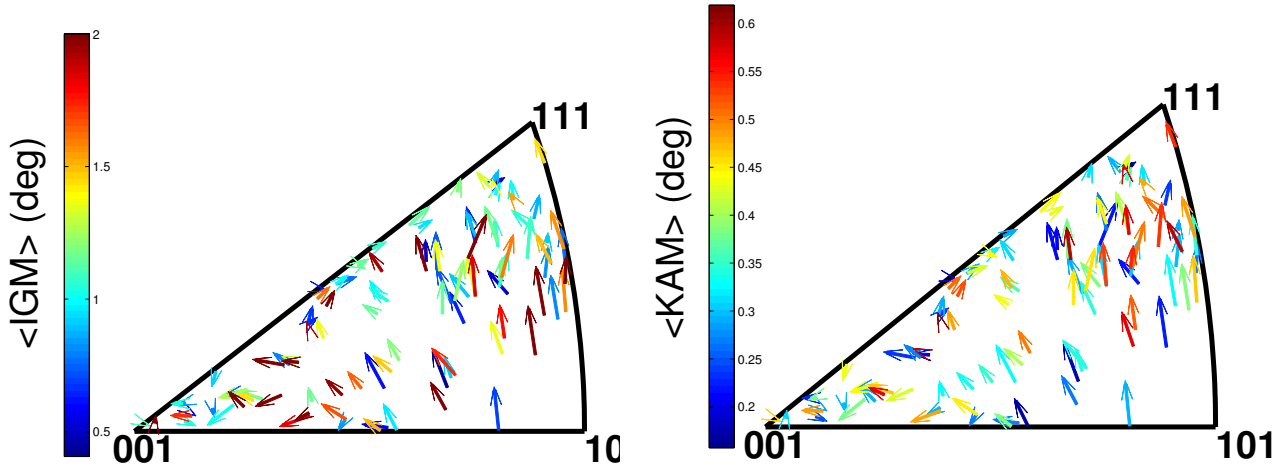

(a) (b)

Figure 3: Lattice reorientation from initial to 14% strain, as shown in Fig. 2, but now colored by (a) ⟨IGM⟩ and expanded color scale is used, where maximum ⟨IGM⟩ was 2.9956° and (b) ⟨KAM⟩. The grain average values for both quantities are computed in the 14% strain state. No obvious correlation is seen between ⟨IGM⟩ or ⟨KAM⟩ and the initial orientation.

not be detected in either the raw or reduced experimental diffraction images. Thus, we use KAM as a measure of local disorder on the length scale of the experimental and reconstruction spatial resolution and recommend caution in using it as a measure of microscopic orientation gradients.

Fig. 3(a) makes it clear that ⟨IGM⟩ is essentially uncorrelated with ⟨**g**⟩, and similar behavior is seen for ⟨KAM⟩ from fig. 3(b). This is consistent with the idea that grain breakup, being outside the context of any classical, say, Taylor, model, is dominated by local effects associated with specific microstructural neighborhoods and the associated localized reorientations of stress fields. A simple example of this was shown by Kanjarla *et al.* [113]. Employing CPFEM simulations of columnar grains, they demonstrated that simply altering the orientation of a neighboring grain (and consequently the local deformation fields) was sufficient to suppress grain fragmentation. While observation of mosaic structures through broadening of diffraction patterns is an old subject [114], the recognition of its origins in locally driven stress patterns associated with plasticity is not so well recognized.

7.4. Spatial Distribution of Orientation

Motivated by the examples in the literature of comparisons of orientation spread [85, 19, 89], we illustrate the spatial distribution of lattice re-orientations for two grains in Figs. 4 and 5. Owing to the limitation of 2-D measurements and to material deformation and flow, the measured cross-sections at different strain levels do not contain exactly the same pixels. The gaps within the grains are due to the intrusion of annealing twins and grains that are centered in other sample cross-sections but that extend into the measured one. The pictured grains (grains 2 and 15) are pointed out in Fig. 1 and their orientation evolution is emphasized in Fig. 2. Since Figs. 4 and 5 map orientation differences, detail that is not apparent in Fig. 1 is easily seen here. In the initial, essentially unstrained and well annealed state, little variation is visible even in the difference plots since the grains are very well ordered. Even here, however, subtle structure is visible in the KAM maps: many closed loops of slightly increased orientation differences ($\sim 0.15°$) are present. Higher orientation resolution (using integration intervals $\delta\omega < 1°$) would be required to reliably interpret such structures.

With increased strain, we see the distinct behaviors implied by Fig. 2. Grain 15 develops regions of distinct orientation whereas grain 2 exhibits rather homogeneous orientation noise that is only slightly distinguishable in the IGM and KAM maps. While the local orientation differences in the KAM maps cannot be interpreted as being simply related to orientation gradients, they do demonstrate that qualitatively distinct behaviors are seen in the two grains. The IGM maps are easily interpreted as illustrating the existence of domains of subtly distinct orientations, particularly in grain 15; these domains are surrounded by low angle grain boundaries as is clear from the corresponding KAM map.

In contrast to expectations, both grain maps suggest that KAM is reduced near the perimeter of the

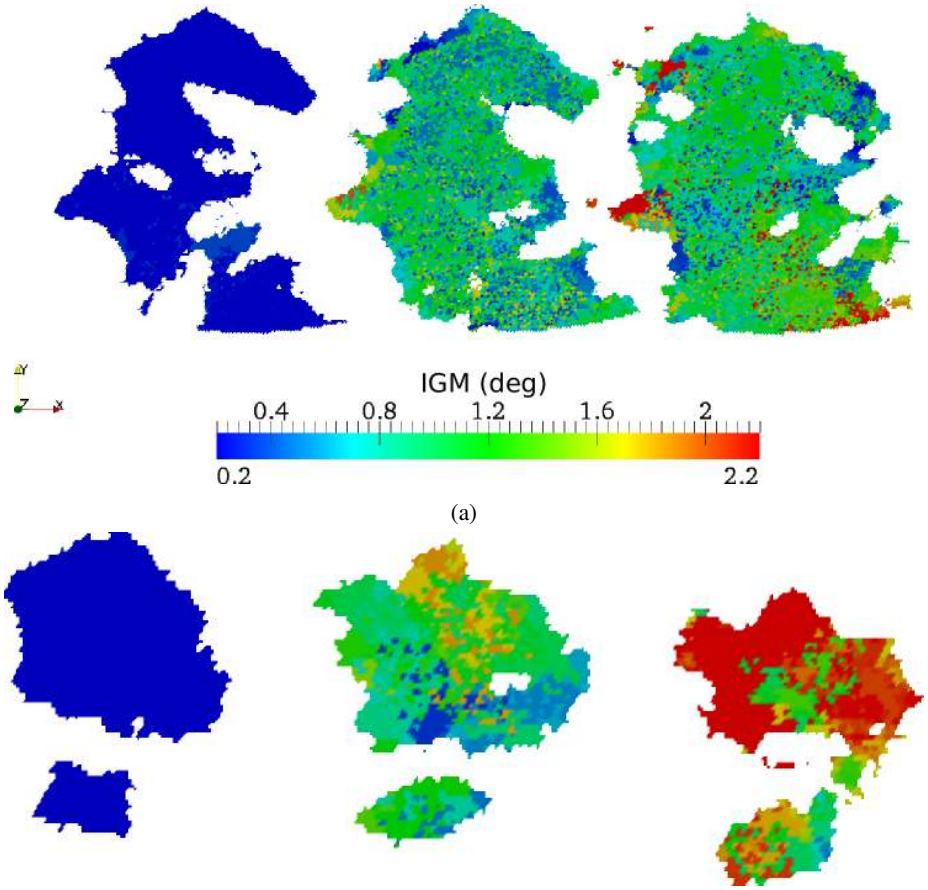

Figure 4: IGM maps at 0.06%, 7%, and 14% tensile strains (left to right) for (a) grain 2 and (b) grain 15.

grains in both 7% and 14% strain states. The caveats given above on nf-HEDM based KAM interpretation should be reinforced here: the 2.8μm resolution voxels used here are certainly too coarse to reliably probe behavior on micron or lower length scales; the behavior seen in the KAM plots needs to be carefully correlated with observed diffraction signals and such work is underway. Post-mortem EBSD measurements are being performed on this sample [115]. However, with a sub-micron beam size, orientation gradients do appear to increase near boundaries [115].

Fig. 6 shows the average IGM and KAM for all 100 tracked grains versus strain. As expected, the average values increase monotonically with strain [9, 116]. Both long- ($\langle$IGM$\rangle$) and short-range ($\langle$KAM$\rangle$) orientation variations increase with deformation and these measures track each other surprisingly closely. However, heterogeneity of damage accumulation is reflected in the fact that the standard deviations among grains are comparable to the average values. Additional analysis, preferably with fully three dimensional data, is needed to determine the degree to which this heterogeneity is correlated with grain orientation (hard grains resisting deformation) and the degree to which local stress re-orientation and concentration plays a role.

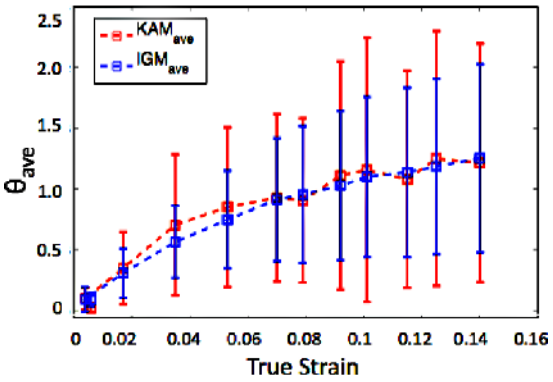

Figure 6: $\langle$IGM$\rangle$ and $\langle$KAM$\rangle$ as a function of strain from 0.06%-14%. The error bars are standard deviations across the 100 largest grains.

7.5. Direct comparison with model predictions

As mentioned above, it should be possible to compute experimentally measured behavior using crystal plasticity with the expectation that good agreement

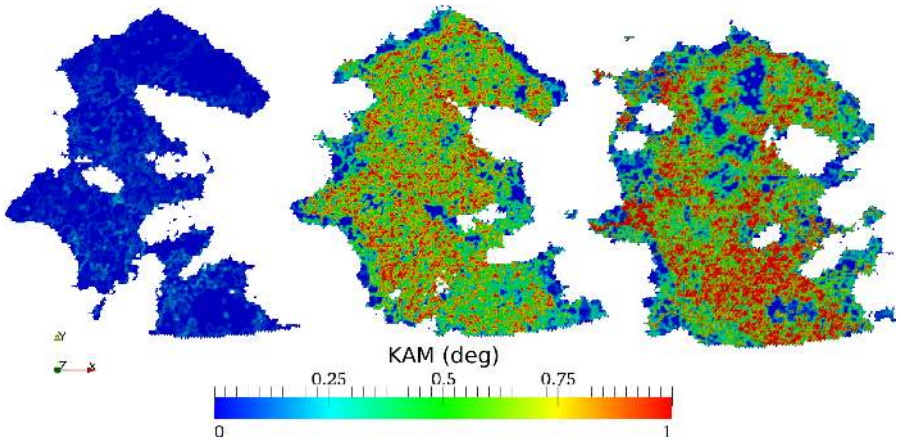

(a)

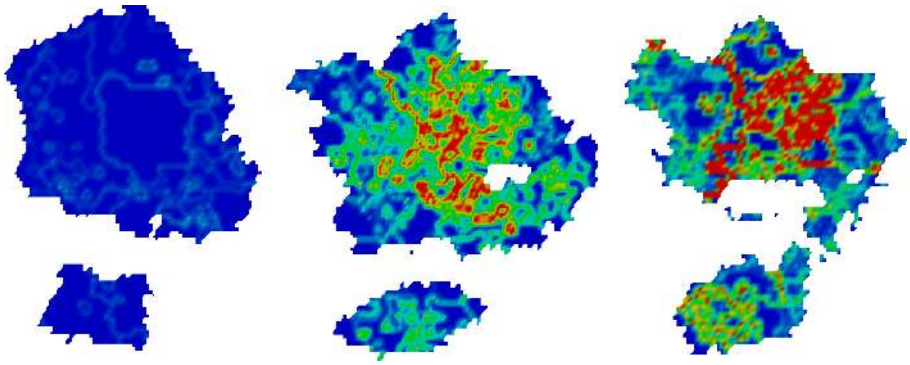

(b)

Figure 5: KAM maps calculated for (a) grain 2 and (b) grain 15 at 0.06%, 7%, and 14% tensile strains (from left to right). To reveal patterns at low KAM values, the color scale saturates at 1°.

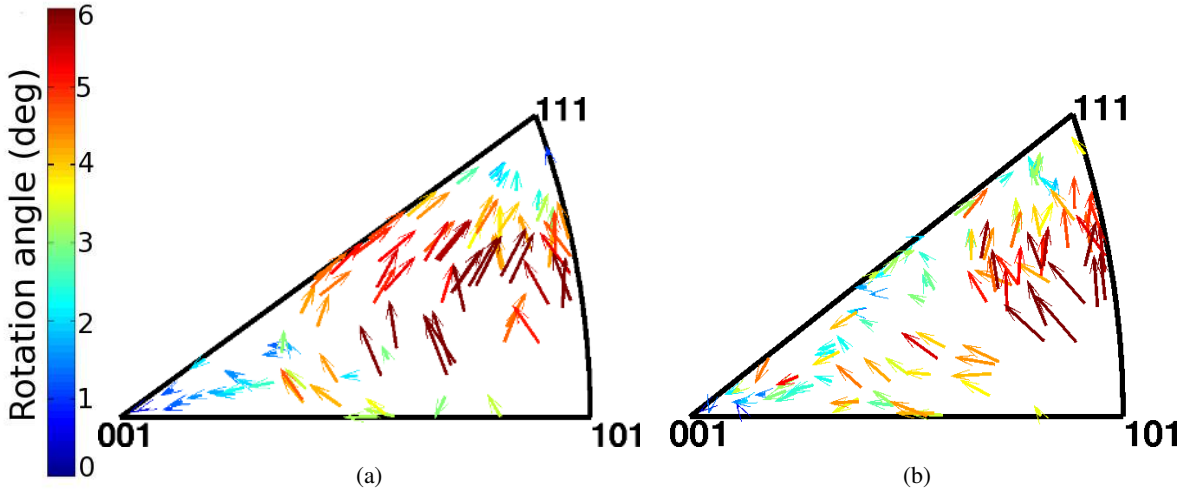

(a) (b)

Figure 7: Inverse pole figures showing predicted lattice rotations using the 100 largest measured grains as the initial state. (a) Rotations of the tensile axis predicted by the Taylor model and (b) rotations obtained from a VPFFT simulation (see text for details). These figures can be directly compared to the experimental rotations of Fig. 2.

validates the computation and discrepancies motivate improvements to methods and constitutive relations. We illustrate this approach using our single cross-section measurements. To help show the effects of interactions between neighboring grains, we consider a classical mean-field or Taylor model [21], which

treats each grain as an isolated case (q.v. section 3.4), and a state-of-the-art computational visco-plastic model that includes interactions between grains and maintains stress equilibrium throughout the polycrystal.

7.5.1. Comparison of Lattice Rotations

Fig. 7a shows the computed lattice rotations in terms of the location of the tensile axis in local crystal coordinates. The dispersion in rotation directions in local regions of the triangle is due to the lack of unique crystal orientation specification in this two dimensional plot and consequent variation in Schmid factors. Note that the orientation change shown in fig. 7a was computed for individual single crystal domain in VPFFT to reproduce the effect of the Taylor model, albeit with the rate sensitive formulation (not the original minimum slip criterion). As in previous work [117], global trends are reasonably comparable to observations but the Taylor model is not quantitative in either rotation angles or directions. A more sophisticated model that includes grain-to-grain interactions as well as additional aspects of modern plasticity models is required.

Going beyond the simple geometric Taylor model requires use of complex plasticity models as described in Sec. 3. We apply the VPFFT code described in Sec. 4 to our measured initial structure shown in Fig. 1a. Since we have measured only a single cross-section, this map is simply extended in the perpendicular direction into a columnar structure. A compliant buffer region is generated around the measured and extruded virtual microstructure so as to allow for the periodic structure assumed in the FFT algorithm. A parameter values in the Voce model, Eq. 3, were chosen so as to match the macroscopic stress-strain curve, which was consistent with previous measurements for fcc copper [118]. The rate-sensitivity exponent is $n = 10$ and $\{111\}\langle 110\rangle$ is the active slip mode. Hardening parameters in the extended Voce law that reproduced the measured stress-strain curve were: $\tau_i^s = 65$ MPa, $\tau_f^s = 45$ MPa, $\theta_i^s = 1230$ MPa, $\theta_f^s = 170$ MPa, $(s = 1, 12)$ and $h^{ss'} = 1$, for all ss'.

Fig. 7(b) shows the lattice reorientations predicted by the VPFFT simulation. Global trends are similar to those of both the experiment and Taylor models. Grain interactions are reflected in numerous significant differences between Fig. 7a and b. However, the degree of one-to-one agreement with the experiment is not significantly improved with some grains showing closer agreement but others being further from the observations than the Taylor model. This is consistent with the results in the literature [19]. Improved agreement may be obtained with a fully three dimensional experimental data set in which all grain neighbors are correctly represented in the model.

With improved overall agreement, it will be important to make more extensive comparisons using the full orientation specification for each grain and to examine the intra-granular behavior reflected in Fig. 2(b).

7.5.2. Comparison of IGM and KAM

In order to address orientation gradients and the effect of neighborhood, local fields predicted by the VPFFT simulation were compared with the experiments, for the same two grains examined in the earlier sections. Fig. 8(a) shows the comparison of the IGM fields between the experiment (left image) and the simulation (right image). Although the magnitude of the misorientation is quite different with larger values in the simulation, qualitatively there are some similarities between the two results. The grain fragmentation is more drastic in the case of grain 15 than in grain 2 in both the results. However, the correlation is not strong enough to draw definitive conclusions. Fig. 8(b) shows the KAM development for the two grains at 14% tensile strain for both experiment (left image) and VPFFT simulation (right image). The experimental maps show a heterogeneous distribution across each grain with smaller values (blue color) at the perimeter. The simulation maps show higher KAM values that are mostly localized near boundaries and little accumulation of gradients in the grain interiors. In the experiment, the gradients most likely correspond to cell structures within the grains, whereas the simulation exhibits banded structures. Further investigations are required to understand the sources of such contradictory behaviors between experiments and simulations.

7.6. Discussion of Cu Tensile Test

Predicting mechanical behavior and effective response of polycrystalline materials undergoing plastic deformation has been one of the main foci of the solid mechanics modeling community [119, 18, 55]. Polycrystal plasticity models are used to predict the crystallographic texture evolution and the anisotropy in the mechanical properties of materials. While their validation is performed through quantitative comparison of the measured and predicted textures such as orientation distribution function (ODF), only rarely are the reorientations at the individual crystallographic levels considered. As commonly observed e.g. by Panchanadeswaran [78] individual grains develop large internal orientation gradients, 2(b). Surface based measurements and lattice reorientation were compared by Lebensohn *et al.*[19] with the FFT based viscoplastic deformation simulations to predict the evolution of microstructure of a polycrystalline Cu specimen under uniaxial tension. The lattice reorientation trend observed in our experiment and predicted by VPFFT simulation from initial to

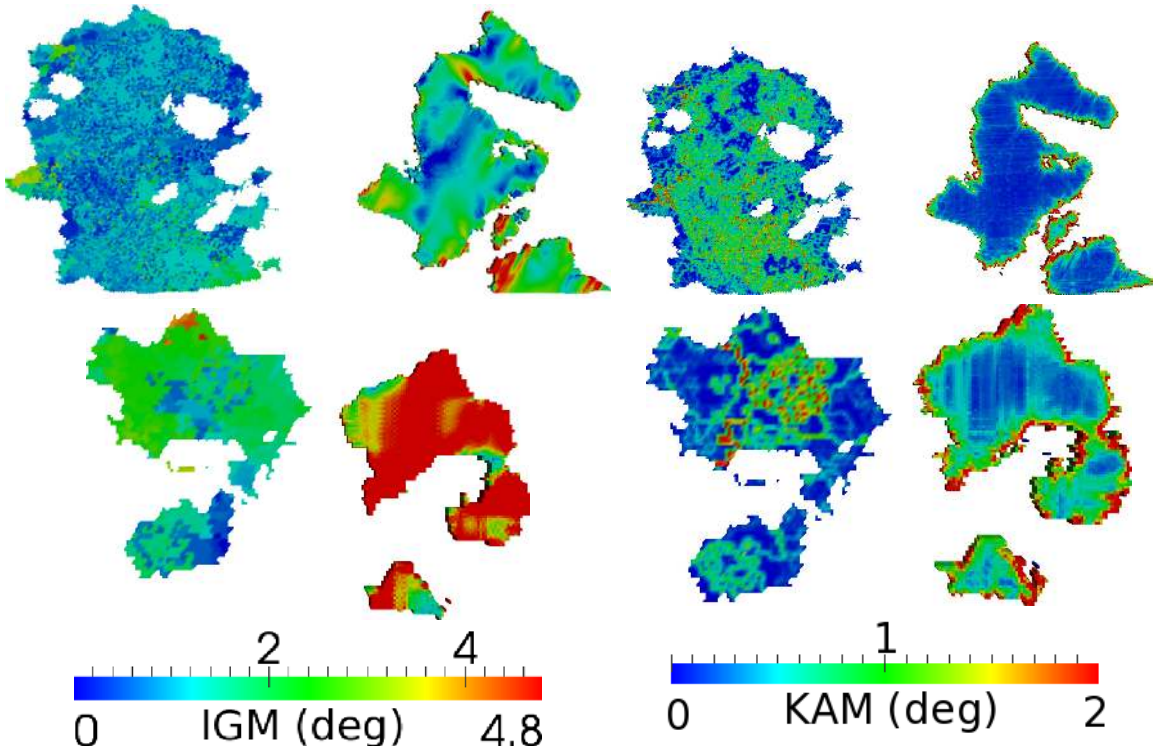

(a) (b)

Figure 8: Misorientation field development for grains 2 (top) and 15 (bottom) extracted from the experiment (left) and VPFFT (right). (a) IGM field development within the grains after 14% tensile deformation. (b) KAM field development within the grains after 14% tensile deformation. The color scales are expanded relative to Figs. 4 and 5 due to the larger predicted rotations obtained from the model.

11% strain qualitatively match with the rotation trajectories observed in figure 2(a). The orientations close to ⟨001⟩ and ⟨111⟩, considered to be stable orientations, exhibited minimum lattice rotations while orientations close to ⟨110⟩ and along ⟨001⟩-⟨111⟩ line showed highest reorientations. More specifically, the original Taylor work used a minimum shear principle to solve for the stress state at any given orientation (relative to the tensile axis). In many parts of the unit triangle there is a range of reorientation directions that are possible. As discussed above, this arises from the ambiguity problem in polycrystal plasticity and is generally resolved by introducing rate sensitivity, which results in a unique solution for the distribution of slips. Nonetheless, it is interesting that the parts of the unit triangle where the most variability in reorientation occur, close to ⟨001⟩ for example, correspond to the largest variation in possible reorientation. Winther *et al.* [108], in common with most authors, presented a comparison of their experimental results with theoretical reorientations based on a unique solution in the Taylor model framework although they suggested that ambiguity (especially near the ⟨001⟩ corner) could account for some of the discrepancies. It is notable that the VPFFT results also show maximum variability in reorientation near ⟨001⟩ and along the ⟨001⟩-⟨111⟩ line. The rotation paths and magnitude of reorientation obtained from the nf-HEDM observations are also consistent with the lattice rotations observed using the 3DXRD technique for average orientation measurements of 100 grains in an Al sample [50]. Concerning the development of intragranular orientation gradients (IGM), Fig. 2, our results do not show any correlation with orientation, which differs from previous results that suggest that the largest gradients are expected for orientations with the maximum divergence, e.g. [19, 94].

8. Conclusions

This paper reviewed comparisons of experimentally measured plastic deformation with numerical simulation results from calculations using crystal plasticity that resolve the fields at the microstructural scale. The invariable conclusion is that reasonable qualitative agreement is found but that there are many differences, both quantitative and qualitative, in the strain field, orientation field (or both) that can be found at the local, grain-scale level. Efforts to model plastic deformation using direct dislocation simula-

tion, as opposed to continuum-scale, were also reviewed; here the conclusion is that the techniques do not have capability to simulate polycrystals although there are indications that it will become possible in the near future. To point toward future capabilities for such comparisons, experimental results from a non-destructive, synchrotron based High Energy Diffraction Microscopy measurement were presented. The in-situ measurement tracked a single layer of microstructure to 14% plastic strain. The experiment was then simulated using an image-based viscoplastic crystal plasticity method (VPFFT). Measurement of heterogeneous orientation fields demonstrated that it is possible to distinguish between grain fragmentation and local dispersion of orientation. Comparison of the experimental evolution with simulations based on the initial state again show good qualitative agreement for average values of grains but marked differences in the local, intra-grain fields. Both the short and long range orientation gradients increase with deformation, and the spatial distributions of IGM and KAM both show heterogeneous defect accumulations. The VPFFT simulations showed good agreement between the predicted lattice rotations and the experiments. In general, however, the magnitudes of reorientation were over-predicted by the model.

2D nf-HEDM measurements can be readily extended to 3D, which are highly likely to improve our understanding of the effect of neighborhood and neighbor interactions on the microstructural evolution, as noted by Zeghadi *et al.* [120]. The major advantage of orientation mapping in 3D with HEDM is the ability to measure microstructural evolution in the interior of materials and thus not be limited to surface observations. On the other hand, resolving orientation gradients requires a spatial resolution finer than that of the dislocation cell (or subgrain) structure that develops during deformation, which HEDM does not accomplish for Cu at room temperature. Fully 3D characterization using nf-HEDM technique will be reported in a later publication.

It is reasonable to ask what would constitute acceptable agreement between experiment and simulation. The difficulty here is that one is comparing tensor fields, such as an orientation map, rather than single values. One measure of difference might be the average pointwise relative error and acceptable agreement could be stated as requiring the error to be less than, say, twenty percent. Another approach would be to define an error bound based on uncertainty analysis of the measurement along with an equivalent uncertainty for simulation based on numerical errors compounded with model uncertainty. Then we suggest that acceptable agreement would be for the comparisons to agree within the combined uncertainties. In fact, it would be substantial progress if one could perform an experiment and a corresponding calculation that showed good qualitative agreement setting aside detailed quantitative differences.

The follow-on question is then what recommendations can be made to advance the two major challenges stated at the outset. One is clearly to hope for advances in theoretical understanding of large populations of dislocations. The second is to recommend that improvements be sought both in the constitutive relations used in continuum-scale simulations (which are likely to remain useful because of their practical utility and scalability), and that improvements in theory be sought including numerical implementation of large-scale dislocation simulations (using either explicit dislocations dynamics or some form of field dislocations mechanics) to enable direct comparison to spatially resolved experiments on polycrystal deformation that span statistically significant volumes of materials. The benefit to be obtained is simulations that are accurate enough to allow us to understand the effect of microstructure on plastic deformation and to be able to predict distributions of fields such as orientation and strain because, for example, the upper tails should predict damage initiation.

Acknowledgements

This research was supported by the US Department of Energy, Office of Basic Energy Sciences, Division of Materials Sciences and Engineering, under award DESC0002001. Use of the Advanced Photon Source was supported by the US Department of Energy, Office of Science, Office of Basic Energy Sciences, under contract No. DE-AC02-06CH11357. Research was also supported in part by the National Science Foundation through XSEDE resources provided by Texas Advanced Computing Center under grant number DMR080072, and in part by the National Energy Research Scientific Computing Center, which is supported by the Office of Science of the U.S. Department of Energy under Contract No. DE-AC02-05CH11231.

[1] JP Hirth and J Lothe. *Theory of Dislocations*. Wiley, 1982.

[2] Y Xiang, D J Srolovitz, L T Cheng, and E Weinan. Level set simulations of dislocation-particle bypass mechanisms. *Acta materialia*, 52:1745–1760, 2004.

[3] UF Kocks, CN Tomé, and H-R Wenk. *Texture and anisotropy: preferred orientations in polycrystals and their effect on materials properties*. Cambridge university press, 2000.

[4] JS Kallend and GJ Davies. A simulation of texture development in fcc metals. *Philosophical Magazine*, 25(2):471–490, 1972.

[5] P Van Houtte, AK Kanjarla, A Van Bael, M Seefeldt, and L Delannay. Multiscale modelling of the plastic anisotropy and deformation texture of polycrystalline materials. *European Journal of Mechanics-A/Solids*, 25(4):634–648, 2006.

[6] UF Kocks, AS Argon, and MF Ashby. Thermodynamics and kinetics of slip. *Prog. Mat. Sci.*, 19:1, 1975.

[7] L. Kubin, B. Devincre, and T. Hoc. Modeling dislocation storage rates and mean free paths in face-centered cubic crystals. *Acta materialia*, 56(20):6040–6049, 2008.

[8] AH Cottrell. *Dislocation and plastic flow in crystals*. Clarendon Press Oxford, 1953.

[9] DA Hughes, Q Liu, DC Chrzan, and N Hansen. Scaling of microstructural parameters: misorientations of deformation induced boundaries. *Acta Materialia*, 45(1):105–112, 1997.

[10] RA LeSar. Simulations of dislocation structure and response. *Annual Reviews of Condensed Matter Physics*, 2013. in press.

[11] A Acharya. Microcanonical entropy and mesoscale dislocation mechanics and plasticity. *Journal of Elasticity*, 104(1-2):23–44, 2011. SI.

[12] I Groma. Statistical physical approach to describe the collective properties of dislocations. In R Pippan and P Gumbsch, editors, *Multiscale Modelling of Plasticity and Fracture by Means of Dislocation Mechanics*, volume 522, pages 213–270. Springer, Vienna, 2010.

[13] M Zaiser and T Hochrainer. Some steps towards a continuum representation of 3d dislocation systems. *Scripta materialia*, 54(5):717–721, 2006.

[14] J Crabtree and J Sarrao. From quanta to the continuum: Opportunities for mesoscale science. Technical report, Basic Energy Sciences Advisory Committee (BESAC), 2012.

[15] GW Crabtree and JL Sarrao. Opportunities for mesoscale science. *Mater. Res. Soc. Bulletin*, 37:1079, 2012.

[16] L Lei, JL Marin, and M Koslowski. Phase-field modeling of defect nucleation and propagation in domains with material inhomogeneities. *Modelling and Simulation in Materials Science and Engineering*, 21(2), 2013. 025009.

[17] SF Li, J Lind, CM Hefferan, R Pokharel, U Lienert, AD Rollett, and RM Suter. Three-dimensional plastic response in polycrystalline copper via near-field high-energy x-ray diffraction microscopy. *Journal of Applied Crystallography*, 45(6):0–0, 2012.

[18] RA Lebensohn. N-site modeling of a 3d viscoplastic polycrystal using fast fourier transform. *Acta Materialia*, 49(14):2723–2737, 2001.

[19] RA Lebensohn, R Brenner, O Castelnau, and AD Rollett. Orientation image-based micromechanical modelling of subgrain texture evolution in polycrystalline copper. *Acta materialia*, 56(15):3914–3926, 2008.

[20] R Pokharel, SF Li, J Lind, CM Hefferan, U Lienert, RA Lebensohn, RM Suter, and AD Rollett. Quantifying damage accumulation using state-of-the-art fft method. In *Materials Science Forum*, volume 702, pages 515–518. Trans Tech Publ, 2012.

[21] GI Taylor. Plastic strain in metals. *J. Inst. Metals (U.K.)*, 62:307, 1938.

[22] AD Rollett. Orientation mapping. In DE Laughlin, editor, *Encyclopedia of Physical Metallurgy, 5th Ed.* Elsevier, 2013.

[23] JE Field, NK Bourne, SJP Palmer, SM Walley, and JM Smallwood. Hot-spot ignition mechanisms for explosives and propellants. *Philosophical Transactions Of The Royal Society Of London Series A-Mathematical Physical And Engineering Sciences*, 339(1654):269–283, 1992.

[24] P. J. Miller, C. S. Coffey, and V. F. DeVost. Heating in crystalline solids due to rapid deformation. *Journal of Applied Physics*, 59(3):913–916, 1986.

[25] JM Papazian, EL Anagnostou, SJ Engel, D Hoitsma, J Madsen, RP Silberstein, G Welsh, and JB Whiteside. A structural integrity prognosis system. *Engineering Fracture Mechanics*, 76:620–632, 2009.

[26] See "The Notebooks of Leonardo da Vinci" (1945), Edward McCurdy, London (P. 546); and "Les Manuscrits de Leonard de Vinci", translated in French by C. Ravaisson-Mollien, Institut de France (1881-91), Vol. 3, 1500.

[27] Posthumously edited by M. de la Hire. Traité du mouvement des eaux. Copied from article by ZP Bazant in Fracture Mechanics of Concrete Structures. Proceedings FRAMCOS-3, AEDIFICATO Publishers, D79104 Freiburg, Germany, "Size effect in tensile, compression fracture of concrete structures: computational modeling, and design", 1686.

[28] B Epstein. Application of the theory of extreme values in fracture problems. *Journal of the American Statistical Association*, 43(243):403–412, 1948.

[29] AM Freudenthal and EJ Gumbel. Minimum life in fatigue. *Journal of the American Statistical Association*, 49(267):575–597, 1954.

[30] Y Murakami and S Beretta. Small defects and inhomogeneities in fatigue strength: experiments, models and statistical implications. *Extremes*, 2(2):123–147, 1999.

[31] MA Przystupa, RJ Bucci, PE Magnusen, and AJ Hinkle. Microstructure based fatigue life predictions for thick plate 7050-t7451 airframe alloys. *International journal of fatigue*, 19(93):285–288, 1997.

[32] CP Przybyla and DL McDowell. Microstructure-sensitive extreme-value probabilities of high-cycle fatigue for surface vs. subsurface crack formation in duplex ti–6al–4v. *Acta Materialia*, 60(1):293–305, 2012.

[33] HM Zbib. Advances in discrete dislocations dynamics and multiscale modeling. *Journal of Engineering Materials and Technology*, 131:041209–1, 2009.

[34] VS Deshpande, A Needleman, and E Van der Giessen. Discrete dislocation plasticity modeling of short cracks in single crystals. *Acta Materialia*, 51(1):1–15, 2003.

[35] S Brinckmann and E Van der Giessen. A fatigue crack initiation model incorporating discrete dislocation plasticity and surface roughness. *International Journal of Fracture*, 148(2):155–167, 2007.

[36] F Barbe, L Decker, D Jeulin, and G Cailletaud. Intergranular and intragranular behavior of polycrystalline aggregates. part 1: F.e. model. *International Journal of Plasticity*, 17(4):513–536, 2001. doi: DOI: 10.1016/S0749-6419(00)00061-9.

[37] F Barbe, S Forest, and G Cailletaud. Intergranular and intragranular behavior of polycrystalline aggregates. part 2: Results. *International Journal of Plasticity*, 17(4):537–563, 2001.

[38] O Diard, S Leclereq, G Rousselier, and G Cailletaud. Evaluation of finite element based analysis of 3d multicrystalline aggregates plasticity - application to crystal plasticity model identification and the study of stress and strain fields near grain boundaries. *International Journal of Plasticity*, 21(4):691–722, 2005.

[39] T Kanit, S Forest, I Galliet, V Mounoury, and D Jeulin. Determination of the size of the representative volume element for random composites: statistical and numerical approach. *International Journal Of Solids And Structures*, 40(13-14):3647–3679, 2003.

[40] AC Lewis, C Suh, M Stukowski, AB Geltmacher, K Rajan, and G Spanos. Tracking correlations between mechanical response and microstructure in three-dimensional reconstructions of a commercial stainless steel. *Scripta Materialia*, 58(7):575–578, 2008.

[41] AD Rollett, RA Lebensohn, M Groeber, Y Choi, J Li, and GS Rohrer. Stress hot spots in viscoplastic deformation of polycrystals. *Modelling and Simulation in Materials Science and Engineering*, 18(7):074005, 2010.

[42] D Peirce, RJ Asaro, and A Needleman. An analysis of nonuniform and localized deformation in ductile single crystals. *Acta metallurgica*, 30(6):1087–1119, 1982.

[43] RJ Asaro and A Needleman. Overview no. 42 texture development and strain hardening in rate dependent polycrystals. *Acta metallurgica*, 33(6):923–953, 1985.

[44] GR Canova, UF Kocks, and JJ Jonas. Theory of torsion texture development. *Acta Metallurgica*, 32(2):211–226, 1984.

[45] N. Bertin, L. Capolungo, and I.J. Beyerlein. Hybrid dislocation dynamics based strain hardening constitutive model. *International Journal of Plasticity*, 49:119 – 144, 2013.

[46] CN Tomé and RA Lebensohn. Self consistent homogenization methods for texture and anisotropy. *Continuum Scale Simulation of Engineering Materials: Fundamentals-Microstructures-Process Applications*, pages 473–499,

2004.

[47] P Franciosi. The concepts of latent hardening and strain hardening in metallic single crystals. *Acta Metallurgica*, 33(9):1601–1612, 1985.

[48] F Roters, P Eisenlohr, L Hantcherli, DD Tjahjanto, TR Bieler, and D Raabe. Overview of constitutive laws, kinematics, homogenization and multiscale methods in crystal plasticity finite-element modeling: Theory, experiments, applications. *Acta Materialia*, 58(4):1152–1211, 2010.

[49] UF Kocks. Constitutive behavior based on crystal plasticity. In AK Miller, editor, *Unified Constitutive Equations for Creep and Plasticity*, page 1. Elsevier, New York, 1987.

[50] G Winther, L Margulies, S Schmidt, and HF Poulsen. Lattice rotations of individual bulk grains part ii: correlation with initial orientation and model comparison. *Acta materialia*, 52(10):2863–2872, 2004.

[51] JFW Bishop and R Hill. Xlvi. a theory of the plastic distortion of a polycrystalline aggregate under combined stresses. *Philosophical Magazine*, 42(327):414–427, 1951.

[52] H Moulinec and P Suquet. A numerical method for computing the overall response of nonlinear composites with complex microstructure. *Computer Methods in Applied Mechanics and Engineering*, 157(1):69–94, 1998.

[53] H Moulinec and P Suquet. Comparison of fft-based methods for computing the response of composites with highly contrasted mechanical properties. *Physica B: Condensed Matter*, 338(1):58–60, 2003.

[54] RA Lebensohn, AK Kanjarla, and P Eisenlohr. An elasto-viscoplastic formulation based on fast fourier transforms for the prediction of micromechanical fields in polycrystalline materials. *International Journal of Plasticity*, 32:59–69, 2012.

[55] B Liu, D Raabe, F Roters, P Eisenlohr, and RA Lebensohn. Comparison of finite element and fast fourier transform crystal plasticity solvers for texture prediction. *Modelling and Simulation in Materials Science and Engineering*, 18(8):085005, 2010.

[56] L Allais, M Bornert, T Bretheau, and D Caldemaison. Experimental characterization of the local strain field in a heterogeneous elastoplastic material. *Acta metallurgica et materialia*, 42(11):3865–3880, 1994.

[57] AD Kammers and S Daly. Small-scale patterning methods for digital image correlation under scanning electron microscopy. *Measurement Science and Technology*, 22(12):125501, 2011.

[58] D Raabe, M Sachtleber, Z Zhao, F Roters, and S Zaefferer. Micromechanical and macromechanical effects in grain scale polycrystal plasticity experimentation and simulation. *Acta materialia*, 49(17):3433–3441, 2001.

[59] AJ Schwartz. *Electron backscatter diffraction in materials science*. Springer, 2009.

[60] N Allain-Bonasso, F Wagner, S Berbenni, and DP Field. A study of the heterogeneity of plastic deformation in if steel by ebsd. *Materials Science and Engineering: A*, 2012.

[61] HF Poulsen. *Three-dimensional X-ray diffraction microscopy: mapping polycrystals and their dynamics*, volume 205. Springer, 2004.

[62] HF Poulsen, SF Nielsen, EM Lauridsen, Søren Schmidt, RM Suter, U Lienert, L Margulies, T Lorentzen, and D Juul Jensen. Three-dimensional maps of grain boundaries and the stress state of individual grains in polycrystals and powders. *Journal of applied crystallography*, 34(6):751–756, 2001.

[63] HF Poulsen and S Schmidt. Reconstruction of grain boundaries in polycrystals by filtered back-projection of diffraction spots. *Journal of applied crystallography*, 36(2):319–325, 2003.

[64] W Ludwig, P Reischig, A King, M Herbig, EM Lauridsen, G Johnson, TJ Marrow, and JY Buffiere. Three-dimensional grain mapping by x-ray diffraction contrast tomography and the use of friedel pairs in diffraction data analysis. *Review of Scientific Instruments*, 80(3):033905–033905, 2009.

[65] JV Bernier, NR Barton, U Lienert, and MP Miller. Far-field high-energy diffraction microscopy: a tool for intergranular orientation and strain analysis. *The Journal of Strain Analysis for Engineering Design*, 46(7):527–547, 2011.

[66] CM Hefferan, SF Li, J Lind, U Lienert, AD Rollett, and RM Suter. In situ observation of recovery and grain growth in high purity aluminum. In *Materials Science Forum*, volume 715, pages 447–454. Trans Tech Publ, 2012.

[67] D Juul Jensen and S Schmidt. Time evolution in 3d metal microstructures–recrystallization. *Materials transactions*, 50(7):1655, 2009.

[68] J Oddershede, S Schmidt, HF Poulsen, HO Sorensen, J Wright, and W Reimers. Determining grain resolved stresses in polycrystalline materials using three-dimensional x-ray diffraction. *Journal of Applied Crystallography*, 43(3):539–549, 2010.

[69] RM Suter, D Hennessy, C Xiao, and U Lienert. Forward modeling method for microstructure reconstruction using x-ray diffraction microscopy: Single-crystal verification. *Review of scientific instruments*, 77(12):123905–123905, 2006.

[70] RM Suter, CM Hefferan, SF Li, D Hennessy, C Xiao, U Lienert, and B Tieman. Probing microstructure dynamics with x-ray diffraction microscopy. *Journal of Engineering Materials and Technology*, 130:021007–1, 2008.

[71] SF Li and RM Suter. Adaptive reconstruction method for three-dimensional orientation imaging. *Journal of Applied Crystallography*, 46(2):512–524, 2013.

[72] DP Field, KR Magid, IN Mastorakos, JN Florando, DH Lassila, and JW Morris Jr. Mesoscale strain measurement in deformed crystals: A comparison of x-ray microdiffraction with electron backscatter diffraction. *Philosophical Magazine*, 90(11):1451–1464, 2010.

[73] CM Hefferan, J Lind, SF Li, U Lienert, AD Rollett, and RM Suter. Observation of recovery and recrystallization in high-purity aluminum measured with forward modeling analysis of high-energy diffraction microscopy. *Acta Materialia*, 60(10):4311–4318, 2012.

[74] H Bart-Smith, A-F Bastawros, DR Mumm, AG Evans, DJ Sypeck, and HNG Wadley. Compressive deformation and yielding mechanisms in cellular al alloys determined using x-ray tomography and surface strain mapping. *Acta Materialia*, 46(10):3583–3592, 1998.

[75] W Tong. Detection of plastic deformation patterns in a binary aluminum alloy. *Experimental Mechanics*, 37(4):452–459, 1997.

[76] A Tatschl and O Kolednik. A new tool for the experimental characterization of micro-plasticity. *Materials Science and Engineering: A*, 339(1):265–280, 2003.

[77] R Becker and S Panchanadeeswaran. Effects of grain interactions on deformation and local texture in polycrystals. *Acta metallurgica et materialia*, 43:2701–2719, 1995.

[78] S Panchanadeeswaran, RD Doherty, and R Becker. Direct observation of orientation change by channel die compression of polycrystalline aluminum - use of a split sample. *Acta Materialia*, 44(3):1233–1262, 1996.

[79] C Lineau, C Rey, and P Viaris de Lesegno. Experimental analysis of plastic deformation of steel grains comparison with polycrystal models predictions. *Materials Science and Engineering: A*, 234:853–856, 1997.

[80] F Delaire, JL Raphanel, and C Rey. Plastic heterogeneities of a copper multicrystal deformed in uniaxial tension: Experimental study and finite element simulations. *Acta materialia*, 48(5):1075–1087, 2000.

[81] T Hoc and C Rey. Effect of the free surface on strain localization in mild steel. *Scripta materialia*, 42(11):1053–1058, 2000.

[82] A Tatschl and O Kolednik. On the experimental characterization of crystal plasticity in polycrystals. *Materials Science and Engineering: A*, 356(1):447–463, 2003.

[83] K-S Cheong and EP Busso. Effects of lattice misorientations

on strain heterogeneities in fcc polycrystals. *Journal of the Mechanics and Physics of Solids*, 54(4):671–689, 2006.

[84] Z Zhao, M Ramesh, D Raabe, AM Cuitino, and R Radovitzky. Investigation of three-dimensional aspects of grain-scale plastic surface deformation of an aluminum oligocrystal. *International Journal of Plasticity*, 24(12):2278–2297, 2008.

[85] T. E. Buchheit, G. W. Wellman, and C. C. Battaile. Investigating the limits of polycrystal plasticity modeling. *International Journal of Plasticity*, 21(2):221–249, 2005.

[86] C Rehrl, B Völker, S Kleber, T Antretter, and R Pippan. Crystal orientation changes: a comparison between a crystal plasticity finite element study and experimental results. *Acta Materialia*, 60(5):2379–2386, 2012.

[87] T-Y Wu, JL Bassani, and C Laird. Latent hardening in single crystals i. theory and experiments. *Proceedings of the Royal Society of London. Series A: Mathematical and Physical Sciences*, 435(1893):1–19, 1991.

[88] JL Bassani and T-Y Wu. Latent hardening in single crystals ii. analytical characterization and predictions. *Proceedings of the Royal Society of London. Series A: Mathematical and Physical Sciences*, 435(1893):21–41, 1991.

[89] YS Choi, MA Groeber, PA Shade, TJ Turner, JC Schuren, DM Dimiduk, MD Uchic, C Woodward, AD Rollett, and TA Parthasarathy. Crystal plasticity finite element method simulations for a polycrystalline ni micro-specimen deformed in tension. *Experimental mechanics*, submitted, 2013.

[90] D Raabe, M Sachtleber, Z Zhao, F Roters, and S Zaefferer. Micromechanical and macromechanical effects in grain scale polycrystal plasticity experimentation and simulation. *Acta materialia*, 49(17):3433–3441, 2001.

[91] S Zaefferer, JC Kuo, Z Zhao, M Winning, and D Raabe. On the influence of the grain boundary misorientation on the plastic deformation of aluminum bicrystals. *Acta materialia*, 51(16):4719–4735, 2003.

[92] A Ma, F Roters, and D Raabe. On the consideration of interactions between dislocations and grain boundaries in crystal plasticity finite element modeling - theory, experiments, and simulations. *Acta materialia*, 54(8):2181–2194, 2006.

[93] A Ma, F Roters, and D Raabe. A dislocation density based constitutive model for crystal plasticity fem including geometrically necessary dislocations. *Acta materialia*, 54(8):2169–2179, 2006.

[94] R Quey, PR Dawson, and JH Driver. Grain orientation fragmentation in hot-deformed aluminium: Experiment and simulation. *Journal of the Mechanics and Physics of Solids*, 60(3):509–524, 2012.

[95] L Wang, RI Barabash, Y Yang, TR Bieler, MA Crimp, P Eisenlohr, W Liu, and GE Ice. Experimental characterization and crystal plasticity modeling of heterogeneous deformation in polycrystalline alpha-ti. *Metallurgical And Materials Transactions A-Physical Metallurgy And Materials Science*, 42A(3):626–635, 2011. Symposium on Cost Affordable Titanium III held at the 2010 TMS Annual Meeting FEB 14-18, 2010 Seattle, WA Minerals, Met & Mat Soc.

[96] GE Ice and BC Larson. 3d x-ray crystal microscope. *Advanced Engineering Materials*, 2(10):643–646, 2000.

[97] GB Sarma and PR Dawson. Effects of interactions among crystals on the inhomogeneous deformations of polycrystals. *Acta materialia*, 44(5):1937–1953, 1996.

[98] U Lienert, T-S Han, J Almer, PR Dawson, T Leffers, L Margulies, SF Nielsen, HF Poulsen, and Søren Schmidt. Investigating the effect of grain interaction during plastic deformation of copper. *Acta materialia*, 52(15):4461–4467, 2004.

[99] MP Miller, JS Park, PR Dawson, and TS Han. Measuring and modeling distributions of stress state in deforming polycrystals. *Acta Materialia*, 56(15):3927–3939, 2008.

[100] J Lind. *In-situ High-Energy Diffration Mirosopy Study of Zironium Under Uniaxial Tensile Deformation*. PhD thesis, Carnegie Mellon University, 2013.

[101] R Pokharel. *Spatially resolved in-situ study of plastic deformation in polycrystalline copper using high-energy X-rays and full-field simulations.* PhD thesis, Carnegie Mellon University, 2013.

[102] U Lienert, SF Li, CM Hefferan, J Lind, RM Suter, JV Bernier, NR Barton, MC Brandes, MJ Mills, MP Miller, et al. High-energy diffraction microscopy at the advanced photon source. *JOM Journal of the Minerals, Metals and Materials Society*, 63(7):70–77, 2011.

[103] J Lind, SF Li, R Pokharel, U Lienert, AD Rollett, and RM Suter. Tensile twin nucleation events coupled to neighboring slip observed in 3d. *Submitted*, 2013.

[104] N Christodoulou and JJ Jonas. Work hardening and rate sensitivity material coefficients for ofhc cu and 99.99% al. *Acta Met.*, 32:1655–1668, 1984.

[105] CM Hefferan, SF Li, J Lind, U Lienert, AD Rollett, P Wynblatt, and RM Suter. Statistics of high purity nickel microstructure from high energy x-ray diffraction microscopy. *Computers, Materials, & Continua*, 14(3):209–220, 2010.

[106] CM Hefferan, SF Li, U Lienert, and RM Suter. Observation of annealing of grains in high purity aluminum using high energy x-ray diffraction microscopy. *Bulletin of the American Physical Society*, 54, 2009.

[107] JH Cho, AD Rollett, and KH Oh. Determination of volume fractions of texture components with standard distributions in euler space. *Metallurgical And Materials Transactions A-Physical Metallurgy And Materials Science*, 35A(3A):1075–1086, 2004.

[108] G Winther. Slip systems extracted from lattice rotations and dislocation structures. *Acta materialia*, 56(9):1919–1932, 2008.

[109] HA Padilla, CD Smith, J Lambros, AJ Beaudoin, and IM Robertson. Effects of deformation twinning on energy dissipation in high rate deformed zirconium. *Metallurgical and Materials Transactions A*, 38(12):2916–2927, 2007.

[110] L Margulies, G Winther, and HF Poulsen. In situ measurement of grain rotation during deformation of polycrystals. *Science*, 291(5512):2392–2394, 2001.

[111] TJ Turner and SL Semiatin. Modeling large-strain deformation behavior and neighborhood effects during hot working of a coarse-grain nickel-base superalloy. *Modelling Simul. Mater. Sci. Eng.*, 19:065010, 2011.

[112] J Jiang, TB Britton, and AJ Wilkinson. Measurement of geometrically necessary dislocation density with high resolution electron backscatter diffraction: Effects of detector binning and step size. *Ultramicroscopy*, 2012.

[113] AK Kanjarla, L Delannay, and P Van Houtte. Finite element study of intragrain plastic heterogeneity near a triple junction. *Metallurgical and Materials Transactions A*, 42(3):660–668, 2011.

[114] BE Warren. *X-ray Diffraction*. Dover Press, 1969.

[115] S. subedi, private communication (2013).

[116] C. C. Merriman, D. P. Field, and P. Trivedi. Orientation dependence of dislocation structure evolution during cold rolling of aluminum. *Materials Science and Engineering A*, 494(1-2):28–35, 2008. Symposium on Advances in Microstructure-Based Modeling and Characterization of Deformation Microstructures held at 2007 TMS Annual Meeting FEB 26-28, 2007 Orlando, FL Minerals, Metals, Mat. Soc.

[117] J Oddershede, S Schmidt, HF Poulsen, L Margulies, J Wright, M Moscicki, W Reimers, and G Winther. Grain-resolved elastic strains in deformed copper measured by three-dimensional x-ray diffraction. *Materials Characterization*, 62:651–660, 2011.

[118] C Tome, GR Canova, UF Kocks, N Christodoulou, and JJ Jonas. The relation between macroscopic and microscopic strain hardening in fcc polycrystals. *Acta Met.*, 32:1637–1653, 1984.

[119] SR Kalidindi, A Bhattacharyya, and RD Doherty. Detailed analyses of grain–scale plastic deformation in colum-

nar polycrystalline aluminium using orientation image mapping and crystal plasticity models. *Proceedings of the Royal Society of London. Series A: Mathematical, Physical and Engineering Sciences*, 460(2047):1935–1956, 2004.

[120] A Zeghadi, F N'guyen, S Forest, A-F Gourgues, and O Bouaziz. Ensemble averaging stress–strain fields in polycrystalline aggregates with a constrained surface microstructure–part 1: Anisotropic elastic behaviour. *Philosophical Magazine*, 87(8-9):1401–1424, 2007.

Table 1: Glossary of Terms

Burgers vector	Closure failure around a dislocation, generally a close-packed direction in the crystal.
Slip direction	Unit vector parallel to the Burgers vector.
Slip plane	Glide plane for conservative motion of dislocations, generally a close-packed plane.
Slip system	Combination of slip direction and plane defining the shear strain resulting from dislocation motion.
Orientation (**g**)	By imposing a reference frame on a polycrystalline specimen, the orientation at any point can be defined a proper rotation that brings the frame associated with the lattice into coincidence with the reference frame.
Grain, crystallite	Distinct, approximately compact region in a polycrystal, within which a single lattice orientation can be identified.
Texture	Texture is equivalent to Crystallographic Preferred Orientation i.e. the extent to which grains exhibit a preference for certain orientations (relative to the reference or sample frame).
Misorientation	Minimum rotation angle (and, sometimes, associated axis) required to bring the two lattices on either side of a boundary into coincidence.
Orientation gradient	This refers to gradients in lattice orientation.
Grain boundary	Homophase interface between any pair of grains or crystallites.
Low angle grain boundary	Grain boundary that can be constructed from dislocations whose cores do not overlap
High angle grain boundary	Grain boundary across which the minimum rotation for coincidence of the lattices is larger than the maximum for a low angle boundary.
Subgrain	Distinct, approximately compact region in a polycrystal, within which a single lattice orientation can be identified and which is delimited by (mostly) low angle grain boundaries.
Intra-granular misorientation (IGM)	For each point within a given grain, the IGM value is the magnitude of the misorientation between the orientation at that point and the average orientation for the grain. It is useful for quantifying orientation gradients within grains.
Kernel average misorientation (KAM)	For each point, the KAM is the average of the misorientations between that point and a kernel of points around it. The kernel may vary in extent but here we use nearest neighbor points only. KAM is useful for quantifying the local mosaic spread.
Scanning electron microscope (SEM)	electron microscope commonly used for materials characterization, especially in conjunction with EBSD (qv).
Electron Back-scatter Diffraction (EBSD)	Method used in an SEM to capture and index electron diffraction patterns which in its automated form enables orientation mapping of a suitably prepared surface, see [22].
High-energy diffraction microscopy (HEDM)	Synchrotron-based method for orientation mapping in three dimensions that uses high energy monochromatic x-rays, see [22].
Damage initiation	Damage initiation occurs when a void or a crack is formed in what was fully dense material.
Schmid factor, m	Geometric factor that resolves far field stress, σ, onto a local slip system as shear stress, τ.

Table 1: Glossary of Terms

Taylor model, M	Standard model based on [21] commonly used to simulate texture development and plastic anisotropy; it assumes uniform strain rate and ignores interactions between grains.
Crystal plasticity (CP)	Standard model for continuum scale simulation of solids deforming by dislocation slip (and sometimes also twinning), see Eq. 2.
Finite element method (FEM)	Continuum scale simulation method in which the deforming body is discretized by dividing it up into units each of which has a simple geometrical shape but variable size (and perhaps geometry), each of which is treated as a homogeneously deforming element. CPFEM denotes the variant of FEM that uses crystal plasticity as the constitutive relation between stress and strain rate.
FFT method	In the context of this paper, the FFT method is an image-based algorithm that relies on Fast Fourier Transforms for solving the same equations of equilibrium and compatibility as the FEM accomplishes. VPFFT denotes the viscoplastic version of the algorithm.
Discrete Dislocation Dynamics	Simulation method that operates on ensembles of dislocations represented by discrete line segments with forces defined by elastic interactions and advances in time by integrating the equations of motion.
Molecular Dynamics	Simulation method that operates on an ensemble of atoms with defined (empirical) interaction potentials and advances in time by integrating the equations of motion.

Table 2: Measured nf-HEDM cross-sections at different true strain levels and their corresponding stress (MPa) values.

	S0	S1	S2	S3	S4	S5	S6	S7	S8	S9	S10	S11
ϵ	0.06%	0.4%	1.7%	3.5%	5.3%	7.0%	7.9%	9.2%	10.1%	11.5%	12.5%	14.0%
τ	46.8	69.8	104.3	125.2	146.4	168.1	179.3	187.1	197.9	204.5	214.9	221.3